Mizoguchi-Araake for helping me to establish the anti-fibrin mAb and Mrs. K. Shiina for preparation of this paper.

## References

[1] Y. Matsumura, H. Maeda, A new concept for macromolecular therapeutics in cancer chemotherapy: mechanism of tumoritropic accumulation of proteins and the antitumor agent smancs, Cancer Res. 46 (1986) 6387–6392.
[2] R. Duncan, The dawning era of polymer therapeutics, Nat. Rev. 2 (2003) 347–360.
[3] H. Maeda, Y. Matsumura, EPR effect based drug design and clinical outlook for enhanced cancer chemotherapy, Adv. Drug Deliv. Rev. 63 (2011) 129–192.
[4] F.C. Courtice, The origin of lipoprotein in lymph, in: H.S. Meyersen (chairman), Lymph and the lymphatic system, C.C Thomas, Springfield, IL, 1963, pp. 89–126.
[5] K. Iwai, H. Maeda, T. Konno, Use of oily contrast medium for selective drug targeting to tumor: enhanced therapeutic effect and X-ray image, Cancer 44 (1984) 2115–2121.
[6] T. Tammela, K. Alitalo, Lymphangiogenesis: molecular mechanisms and future promise, Cell 140 (2010) 460–476.
[7] A.A. Gabison, Pegylated liposomal doxorubicin: metamorphosis of an old drug into a new form of chemotherapy, Cancer Invest. 19 (2001) 424–436.
[8] W.J. Gradishar, S. Tjulandin, N. Davidson, H. Shaw, N. Desai, P. Bhar, M. Hawkins, J. O'Shaughnessy, Phase III trial of nanoparticle albumin-bound paclitaxel compared with polyethylated castor oil-based paclitaxel in women with breast cancer, J. Clin. Oncol. 23 (2005) 7794–7803.
[9] Y. Matsumura, K. Kataoka, Preclinical and clinical studies of anticancer agent-incorporating polymer micelles, Cancer Sci. 100 (2009) 572–579.
[10] R. Duncan, Polymer conjugates as anticancer nanomedicines, Nat. Rev. Cancer 6 (2006) 688–701.
[11] D. Peer, J.M. Karp, S. Hong, O.C. Farokhzad, R. Margalit, R. Langer, Nanocarriers as an emerging platform for cancer therapy, Nat. Nanotechnol. 2 (2007) 751–760.
[12] T.M. Allen, Ligand-targeted therapeutics in anticancer therapy, Nat. Rev. 2 (2002) 750–759.
[13] S.O. Doronina, B.E. Toki, M.Y. Torgov, B.A. Mendelsohn, C.G. Cerveny, D.F. Chance, R.L. DeBlanc, R.P. Gearing, T.D. Bovee, C.B. Siegall, J.A. Francisco, A.F. Wahl, D.L. Meyer, P.D. Senter, Development of potent monoclonal antibody auristatin conjugates for cancer therapy, Nat. Biotechnol. 21 (2003) 778–784.
[14] A.M. Wu, P.D. Senter, Arming antibodies: prospects and challenges for immunoconjugates, Nat. Biotechnol. 23 (2005) 1137–1146.
[15] O. Trédan, C.M. Galmarini, K. Patel, I.F. Tannock, Drug resistance and the solid tumor microenvironment, J. Natl. Cancer Inst. 99 (2007) 1441–1454.
[16] C.M. Ghajar, M.J. Bissell, Extracellular matrix control of mammary gland morphogenesis and tumorigenesis: insights from imaging, Histochem. Cell Biol. 130 (2008) 1105–1118.
[17] A.I. Minchinton, I.F. Tannock, Drug penetration in solid tumors, Nat. Rev. Cancer 6 (2006) 583–592.
[18] H.F. Dvorak, Tumors: wounds that do not heal. Similarities between tumor stroma generation and wound healing, N. Engl. J. Med. 315 (1986) 1650–1659.
[19] A.D. Ricart, A.W. Tolcher, Technology insight: cytotoxic drug immunoconjugates for cancer therapy, Nat. Clin. Pract. Oncol. 4 (2007) 245–255.
[20] Y. Saito, M. Yasunaga, J. Kuroda, Y. Koga, Y. Matsumura, Enhanced distribution of NK012, a polymeric micelle-encapsulated SN-38, and sustained release of SN-38 within tumors can beat a hypovascular tumor, Cancer Sci. 99 (2008) 1258–1264.
[21] D. Mahadevan, D.D. Von Hoff, Tumor-stroma interactions in pancreatic ductal adenocarcinoma, Mol. Cancer Ther. 6 (2007) 1186–1197.
[22] H. Maeda, Y. Matsumura, H. Kato, Purification and identification of (hydroxyprolyl$^3$)-bradykinin in ascitic fluid from a patient with gastric cancer, J. Biol. Chem. 263 (1988) 16051–16054.
[23] Y. Matsumura, M. Kimura, T. Yamamoto, H. Maeda, Involvement of the kinin-generating cascade and enhanced vascular permeability in tumor tissue, Jpn. J. Cancer Res. 79 (1988) 1327–1334.
[24] D.R. Senger, S.J. Galli, A.M. Dvorak, C.A. Peruzzi, V.S. Harvey, H.F. Dvorak, Tumor cells secret a vascular permeability factor that promotes accumulation of ascites fluid, Science 219 (1983) 983–985.
[25] N. Ferrara, K.J. Hillan, H.P. Gerber, W. Novotny, Discovery and development of bevacizumab, an anti-VEGF antibody for treating cancer, Nat. Rev. Drug Discov. 3 (2004) 391–400.
[26] H.F. Dvorak, F.R. Rickles, Malignancy and hemostasis, in: R.W. Colman, V.J. Marder, A.W. Clowes, J.N. George, S.Z. Goldharber (Eds.), Hemostasis and Thrombosis: Basic principles and clinical practice, Fifth ed., LippinCott Williams & Wilkins, Philadelphia, 2006, pp. 851–873.
[27] A. Trousseau, Plegmasia alba dolens, Vol. 3, J.B. Balliere et Fils, Paris, 1865.
[28] P.D. Stein, A. Beemath, F.A. Meyers, E. Skaf, J. Sanchez, R.E. Olson, Incidence of venous thromboembolism in patients hospitalized with cancer, Am. J. Med. 119 (2006) 60–68.
[29] M. Yasunaga, S. Manabe, Y. Matsumura, New concept of cytotoxic immunoconjugate therapy targeting cancer-induced fibrin clots, Cancer Sci. 102 (2011) 1396–1402.
[30] E. Ostermann, P. Garin-Chesa, K.H. Heider, M. Kalat, H. Lamche, C. Puri, D. Kerjaschki, W.J. Rettig, G.R. Adolf, Effective immunoconjugate therapy in cancer models targeting a serine protease of tumor fibroblasts, Clin. Cancer Res. 14 (2008) 4584–4592.
[31] A. Palumbo, F. Hauler, P. Dziunycz, K. Schwager, A. Soltermann, F. Pretto, C. Alonso, G.F. Hofbauer, R.W. Boyle, D. Neri, A chemically modified antibody mediates complete eradication of tumours by selective disruption of tumour blood vessels, Br. J. Cancer 104 (2011) 1106–1115.
[32] M. Yasunaga, S. Manabe, D. Tarin, Y. Matsumura, Cancer-stromal targeting therapy by cytotoxic immunoconjugate bound to the collagen 4 network in the tumor tissue, Bioconjugate Chem. 22 (2011) 1776–1783.
[33] M.E. Davis, Z.G. Chen, D.M. Shin, Nanoparticle therapeutics: an emerging treatment modality for cancer, Nat. Rev. Drug Discov. 7 (2008) 771–782.
[34] S. Naito, A.C. von Eschenbach, I.J. Fidler, Different growth pattern and biologic behavior of human renal cell carcinoma implanted into different organs of nude mice, J. Natl. Cancer Inst. 78 (1987) 377–385.
[35] M.E. Fallowfield, Blood flow distribution within transplantable tumors in the mouse, Eur. J. Cancer Clin. Oncol. 25 (1989) 1683–1688.
[36] L.M. Ellis, I.J. Fidler, Finding the tumor copycat. Therapy fails, patients don't, Nat. Med. 16 (2010) 974–975.
[37] T. Hawighorst, P. Velasco, M. Streit, Y.K. Hong, T.R. Kyriakides, L.F. Brown, P. Bornstein, M. Detmar, Thrombospondin-2 plays a protective role in multistep carcinogenesis: a novel host anti-tumor defense mechanism, EMBO J. 20 (2001) 2631–2640.
[38] B.N. Rehlaender, M.J. Cho, Antibodies as carrier proteins, Pharm. Res. 15 (1998) 1652–1656.
[39] N.M. Bhowmick, E.G. Neilson, H.L. Moses, Stromal fibroblast in cancer initiation and progression, Nature 432 (2004) 332–337.
[40] G.K. Alderton, Tumor microenvironment: macrophages lead the way, Nat. Rev. Cancer 10 (2010) 162–163.

Please cite this article as: Y. Matsumura, Cancer stromal targeting (CAST) therapy, Adv. Drug Deliv. Rev. (2012), doi:10.1016/j.addr.2011.12.010

EUROPEAN JOURNAL OF CANCER 47 (2011) 2230–2239

available at www.sciencedirect.com

ScienceDirect

journal homepage: www.ejconline.com

# The inhibition of pancreatic cancer invasion-metastasis cascade in both cellular signal and blood coagulation cascade of tissue factor by its neutralisation antibody

*Yohei Saito* [a,b], *Yuki Hashimoto* [a,b], *Jun-ichiro Kuroda* [a], *Masahiro Yasunaga* [a], *Yoshikatsu Koga* [a], *Amane Takahashi* [a], *Yasuhiro Matsumura* [a,b,*]

[a] *Investigative Treatment Division, Research Center for Innovative Oncology, National Cancer Center Hospital East, 6-5-1 Kashiwanoha, Kashiwa, Chiba 277-8577, Japan*

[b] *Laboratory of Cancer Biology, Department of Integrated Biosciences, Graduate School of Frontier Sciences, The University of Tokyo, 5-1-5 Kashiwanoha, Kashiwa, Chiba 277-8562, Japan*

ARTICLE INFO

*Article history:*
Available online 27 May 2011

*Keywords:*
Pancreatic cancer
Tissue factor
Metastasis
Blood coagulation
Matrix metalloproteinase 9

ABSTRACT

Tissue factor (TF), the initiating cell surface receptor for the blood coagulation cascade, plays an important role in malignant transformation of the pancreas, although the precise mechanism remains unresolved. Here, we report that the TF – factor VIIa complex in human pancreatic cancer cells produced a significant amount of MMP-9 and promoted invasion ability *in vitro* and invasion and metastasis *in vivo*. For treatment, we successfully developed an anti-human TF monoclonal antibody that inhibits both cellular signalling and blood coagulation cascade via TF. Invasive capability and MMP-9 expression were significantly reduced by the antibody. The antibody inhibited not only tumour invasion in the orthotopic model, but also haematogenous metastasis in the portal-injection liver metastasis model. In conclusion, the TF-VIIa complex plays an important role in invasion-metastasis by enhancing tumour cell infiltration ability and forming microthrombi. The newly established anti-human TF neutralisation antibody may be useful for the treatment of pancreatic and other invasive cancers.



## 1. Introduction

In cancer invasion and metastasis, the cancer cells degrade the basement membrane and intravasate into lymphatic or blood microvessels. The cells are then transported to a new location and become clogged within the microvessels, proceeding to grow following extravasation.[1] These steps include cancer cell invasion, degradation of the basement membrane and stromal extracellular matrix (ECM), and formation of microthrombi. The matrix metalloproteinase (MMP) family represents important enzymes that degrade ECM and facilitate tumour invasion.[2] Amongst them, MMP-9 is well-known as one of the most important factors in facilitating invasion and metastasis in pancreatic cancer.[3]

Tissue factor (TF), the initiating cell surface receptor for the coagulation cascade, activates factor VIIa. The TF-VIIa complex activates factor X, and consequently this protease cascade forms fibrin clots.[4,5] The relationship between cancer and blood coagulation was initially described by the French surgeon Trousseau.[6] Cancer patients, especially those with pancreatic, stomach, and glioma cancer, often suffer from a state of hypercoagulation and venous thrombosis, leading to

* *Corresponding author:* at: Investigative Treatment Division, Research Center for Innovative Oncology, National Cancer Center Hospital East, 6-5-1 Kashiwanoha, Kashiwa, Chiba 277-8577, Japan. Tel./fax: +81 4 7134 6857.
E-mail address: yhmatsum@east.ncc.go.jp (Y. Matsumura).

0959-8049/$ - see front matter 
doi:10.1016/j.ejca.2011.04.028

patient morbidity and mortality.[7–9] In another study using a fibrinogen-deficient transgenic mouse model, fibrinogen appeared to be an important element of the metastatic potential of circulating tumour cells.[10] Meanwhile, TF plays an important role in not only blood coagulation but also cell signalling in which the TF-VIIa complex phosphorylates extracellular-regulated kinase 1/2 (ERK1/2) via protease-activated receptor-2 (PAR-2).[11] Moreover, its complex promotes the expression of interleukin-8 (IL-8) and invasion in breast cancer cell lines.[12] However, the concrete involvement of TF in tumour invasion-metastasis has not yet been fully evaluated.

Human pancreatic cancer has one of the worst prognoses amongst cancers.[13] Invasion and metastasis advancing beyond the pancreas are typical. Direct invasion to nearby organs, such as the stomach, duodenum, colon, spleen and kidney frequently occurs. Distant metastasis to the liver and peritoneal dissemination are also commonly seen.[14,15] In terms of the relationship between TF and pancreatic cancer, TF expression is an important early event in malignant transformation of the pancreas.[16] TF expression may contribute to the aggressiveness of pancreatic cancer that would stimulate tumour invasiveness, and evaluation of the primary tumour for TF expression may identify patients with a poor prognosis.[17,18]

Therefore, elucidation of the relationship between TF and pancreatic cancer invasion-metastasis may lead to the development of new therapeutic strategies as well as a better understanding of pancreatic cancer biology.

## 2. Materials and methods

### 2.1. Cell lines

Human pancreatic cancer cell lines BxPC3, Panc1, Capan1, and MIA PaCa-2 were purchased from the American Type Culture Collection (Rockville, MD, USA). The cell lines were maintained in Dulbecco's Modified Eagle's Medium supplemented with 10% faetal bovine serum (FBS) (Cell Culture Technologies, Gaggenau-Hoerden, Germany), 100 units/mL streptomycin, and 2 mmol/L L-glutamine (Sigma, St. Louis, MO, USA) in an atmosphere of 5% $CO_2$ at 37 °C.

### 2.2. Immunocytochemistry

Cells ($1 \times 10^5$) were seeded on a 4-well culture slide (BD Biosciences, Bedford, MA, USA), which was incubated for 24 h at 37 °C. Then, after removal of the medium, the sections were rinsed with phosphate buffered saline (PBS) and soaked in 4% paraformaldehyde phosphate buffer solution for 15 min. The sections were then rinsed with PBS, and endogenous peroxidase activity was blocked with a 0.3% hydrogen peroxide solution in 100% methanol for 20 min. After the sections were rinsed with PBS three times for 5 min each, non-specific protein binding was blocked with 5% skim milk (BD, Franklin Lakes, NJ, USA) in PBS for 30 min at room temperature, followed by washing three times with PBS for 5 min. A mouse monoclonal antibody against human TF (Calbiochem, La Jolla, CA, USA) or a rat monoclonal antibody against human TF (established by USA) named as 1849 was added, incubated for 1 h, and rinsed three times with PBS for 5 min each. The sections were incubated for 30 min with EnVision™/HRP (Dako, Glostrup, Denmark) directed against each primary antibody. The sections were rinsed three times with PBS and incubated using the DAB+(3,3-diaminobenzidine tetrahydrochloride) Liquid System (Dako, Glostrup, Denmark) for 30 s. Finally, the sections were rinsed with water and counterstained with haematoxylin solution.

### 2.3. Immunohistochemistry

$10^7$ cells of each pancreatic cancer cell line were injected subcutaneously in 4-week-old female BALB/c nude mice. When the tumour volume reached 300 $mm^3$, tumours were excised from the mice under anaesthetic. Immunohistochemical analysis was conducted as described previously.[19] As a primary antibody, we used the rat monoclonal antibody against human TF that we created. In addition, we used goat anti-rat IgG/HRP (Jackson ImmunoResearch Laboratories, West Grove, PA, USA) as a secondary antibody.

### 2.4. Transfection of BxPC3 cells with TF short hairpin RNA (TF shRNA), green fluorescent protein (GFP), and luciferase

Lentiviral particles were purchased from Sigma–Aldrich. BxPC3 cell suspension (1000 cells/100 μL) was seeded on a 96-well plate, which was incubated for 24 h at 37 °C. After removal of the medium, 100 μL of medium containing hexadimethrine bromide (final concentration of 8 μg/ml) was added to the cells. Viral particles carrying TF shRNA or non-target shRNA (multiplicity of infection (MOI) = 20) were added to the cells. After selecting the infected cells using 2 μg/ml puromycin, we established a TF-knockdown cell line (BxPC3 TFshRNA) and a control cell line (BxPC3 mock). For the detection of micrometastasis and microinvasion in pancreatic orthotopic tumour xenografts, both BxPC3 mock and BxPC3 TFshRNA were infected with viral particles carrying GFP (MOI = 20). In addition, the BxPC3 cell line stably expressing firefly luciferase and YFP mutant Venus ($BxPC3^{Luc}$) was established. In brief, the coding sequence for firefly luciferase and Venus was subcloned into the pIRES vector (Clontech Laboratories, Mountain View, CA, USA). The fragment consists of Luciferase-IRES-Venus generated from the plasmid with the restriction enzymes Nhe1 and Not1. This fragment was subcloned into the pEF6/V5-His vector (Invitrogen, Carlsbad, CA, USA) to generate plasmids of pEF6-Luciferase IRES Venus. BxPC3 were seeded on 6-well plate 24 h before transfection. The cells were transfected with pEF6-Luciferase IRES Venus using Lipofectamine™ LTX with Plus™ Reagent (Invitrogen) according to the manufacturer's instructions, and then incubated for 48 h at 37 °C. The cells were then passaged in medium containing blasticidin (10 μg/ml; InvivoGen, San Diego, CA, USA) to select the blasticidin resistance gene integrated in the pEF6/V5-His plasmids.

### 2.5. Real-time PCR analysis for MMPs and TF

Total RNA was extracted from pancreatic cancer cell lines using the RNeasy Mini Kit (Qiagen, Valencia, CA, USA) according to the manufacturer's instructions. cDNA was synthesised from total RNA using the High Capacity cDNA Reverse Transcription Kit (Applied Biosystems, Foster City, CA, USA) in accordance with

the manufacturer's instructions. We analysed the expression of five genes: *matrix metallopeptidase 2 (MMP-2), matrix metallopeptidase 7 (MMP-7), matrix metallopeptidase 9 (MMP-9)*, TF, and GAPDH as an internal control gene. For all of these genes, we used commercially available TaqMan primers and probe mixture (Applied Biosystems). The reporter dye at the 5′ end of the probe was FAM™, and the quencher dye at the 3′ end was minor groove binder (MGB). Real-time PCR was performed using precycling heat activation at 95 °C for 20 s, followed by 40 cycles of denaturation at 95 °C for 3 s, and annealing/extension at 62 °C for 30 s, in the Applied Biosystems 7500 Fast Real-Time PCR System. Relative quantification of the total RNA in each sample was conducted using the comparative Ct (threshold cycle) method. In this analysis, the formulas for the relative quantification of each of the genes were as follows: (dCT of each gene) = (Ct of each gene) − (Ct of GAPDH), and (Relative quantification of each gene) = $2^{-(\text{dCt of each gene})}$.

### 2.6. TF ELISA assay

TF protein was measured by IMUBIND® Tissue Factor ELISA Kit (American Diagnostica, Greenwich, CT, USA) in accordance with the manufacturer's instructions.

### 2.7. Cell invasion assay

BxPC3 mock and BxPC3 TFshRNA ($2.5 \times 10^4$ cells diluted in 500 μL of serum-free DMEM) were added to the upper wells of a Transwell® 24-well insert coated with Matrigel™ (BD Biosciences) according to the manufacturer's instructions. DMEM with 10% FBS was added to the lower wells. Cells were incubated for 22 h in an atmosphere of 5% $CO_2$ at 37 °C. Cells in the top wells were removed using cotton swabs. Invaded cells were stained and counted in three different viewing fields. In addition, to avoid the effect of factor VIIa in FBS, 500 μL of cell suspension in serum-free high-glucose DMEM was added to the upper wells after they were deprived of serum for 2 h, and high-glucose DMEM supplied with 1% BSA and 0.5% FBS was poured into the lower wells. Factor VIIa and anti-TF antibodies were also added to the lower wells. At the end of 48 h incubation at 5% $CO_2$, 37 °C, the cells in the top wells were removed and invaded cells were counted. Every invasion assay was conducted two times each.

### 2.8. Gelatin zymography

SDS-gelatin zymography was performed with 10% zymogram gel (Invitrogen). Cells ($2 \times 10^5$) were seeded on a 6-well plate and incubated for 24 h at 37 °C. The medium was removed and incubated for 24 h in serum-free DMEM, after which the medium was collected. Tris–Glycine SDS Sample Buffer (Invitrogen) was added and incubated for 30 min at 37 °C. After electrophoresis at 4 °C, the gel was shaken with zymogram renaturing buffer for 30 min. Next, the zymogram renaturing buffer was removed and zymogram developing buffer (Invitrogen) was added and shaken for 30 min. The gel was added to new zymogram developing buffer and was incubated for 30 h at 37 °C. The gel was fixed and then stained with Quick CBB (Wako Chemicals). MMPs were quantified using Image J software.

### 2.9. Effect of anti-TF mAb on invasion and metastasis in nude mice

To assess metastasis and invasion, we established an orthotopic pancreatic cancer mouse model as described previously.[19] Briefly, BxPC3 mock or BxPC3 TFshRNA expressing GFP ($5 \times 10^6$ cells) was injected into the body of the pancreas of nude mice after laparotomy under anaesthesia. The mice were sacrificed 5 weeks after the injection of cancer cells. An OV110 fluorescence microscope (Olympus, Tokyo, Japan) was used to observe several organs and a dissemination score was calculated to evaluate local tumour invasion and distant metastasis as previously described.[20] Tumour dissemination was quantified as follows: every manifestation of tumour infiltration or metastasis was credited with one point. Additional points were awarded for massive local infiltration, multiple metastatic nodules and metastatic nodules >50 $mm^3$. In treatment experiments, mice inoculated with $BxPC3^{Luc}$ or BxPC3 mock expressing GFP cells on Day 0 were treated for seven consecutive days with 1849 mAb (400 μg/mouse) as a TF neutralisation antibody, or PBS as a control. The IVIS imaging system (Caliper Life Sciences, Hopkinton, MA, USA) was used to observe tumour invasion of mice inoculated with $BxPC3^{Luc}$. After 40 days, mice inoculated with cells expressing GFP were sacrificed. A dissemination score was calculated. To assess the inhibition of haematogenous metastasis by anti-TF antibody, we established a portal-injection liver metastasis model. BxPC3 cells expressing luciferase ($5 \times 10^5$ cells) were directly injected into the portal vein after intravenous administration of 1849 mAb (500 μg/mouse) or PBS as a control. The IVIS imaging system was used to detect liver micrometastasis. All animal experiments were performed in compliance with the Guidelines for the Care and Use of Experimental Animals established by the Committee for Animal Experimentation of the National Cancer Center, Japan; these guidelines meet the ethical standards required by law for proper conduct of animal experiments in Japan.

### 2.10. Statistical analysis

Student's t-test was used for the statistical analyses unless otherwise mentioned. $P < 0.05$ was considered significant.

## 3. Results

### 3.1. TF-positive human pancreatic cancer cells, BxPC3, enhance invasion potential in vitro and in vivo

We used the BxPC3 cell line in a series of our experiments because real-time PCR analysis and immunostaining of TF showed that BxPC3 strongly expressed TF amongst the four pancreatic cancer cell lines (Fig. 1A). Then, we examined the status of TF expression for BxPC3 *in vitro* and *in vivo*. Immunostaining revealed TF expression specifically in cancer cells contacting with stromal tissues, namely the invasive front *in vivo*, although TF expression was uniformly observed in all cells *in vitro* (Fig. 1B). To determine if TF affects pancreatic cancer invasion, we established TF-knockdown BxPC3 cell lines. BxPC3 cells were infected with TF shRNA lentivirus (BxPC3 TFshRNA) and non-target shRNA lentivirus (BxPC3

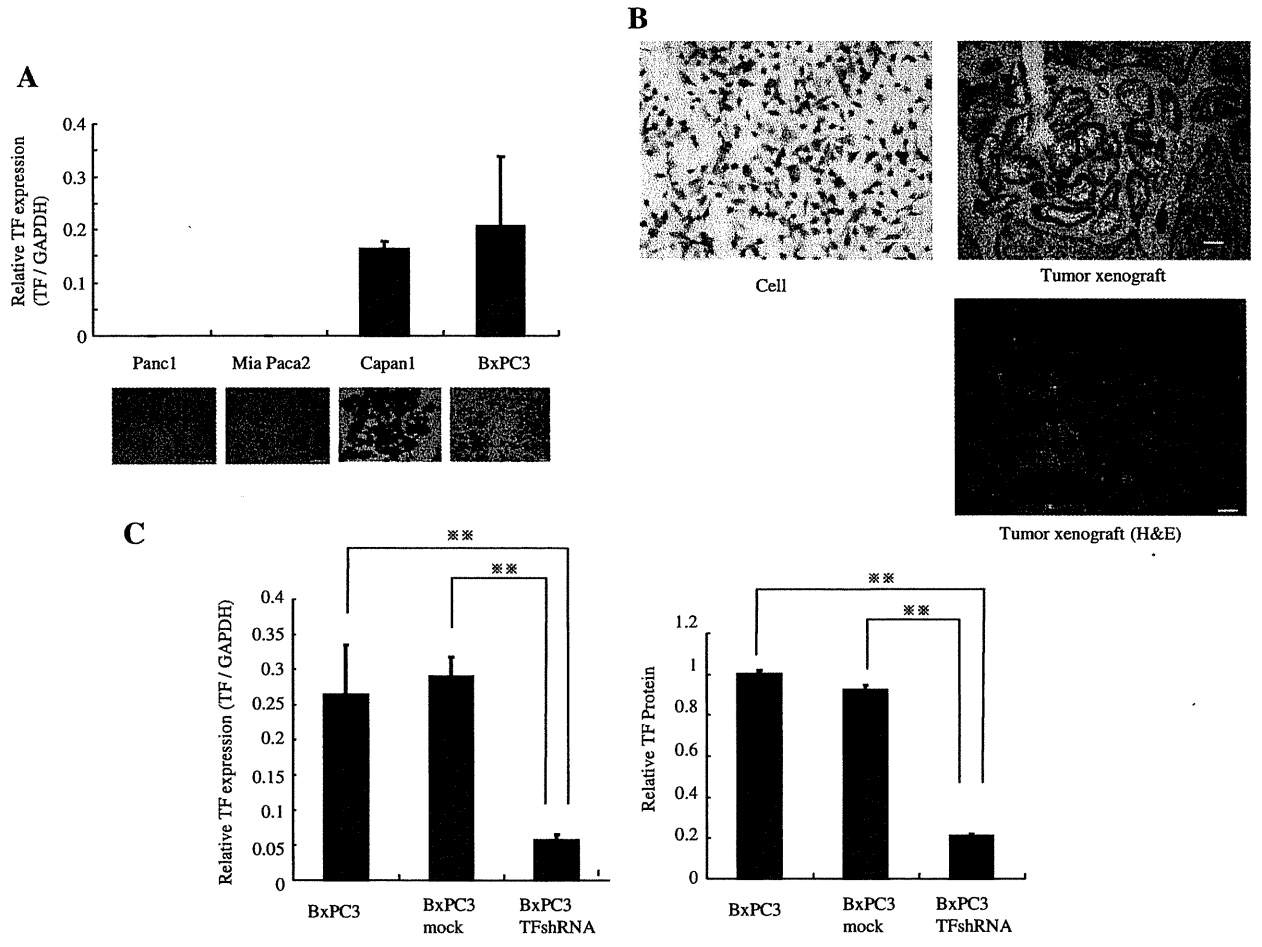


**Fig. 1 – TF knockdown cells decrease the invasion ability. (A) Expression of TF amongst the four human pancreatic cancer cell lines *in vitro*. Total RNA was isolated and mRNA was quantitated by real-time PCR. Data are expressed as the mean ± SD. N = 3–4. The images show the staining of TF. Scale bar 100 μm. (B) Pattern of expression of TF in cultured cells and tumour xenografts. Scale bar 100 μm. T and S mean 'tumour' and 'stroma', respectively. (C) mRNA and protein level of TF in BxPC3, BxPC3 mock and BxPC3 TFshRNA. mRNA was quantitated by real-time PCR and TF protein was quantitated by TF ELISA. Data are expressed as the mean ± SD. N = 3–4. ** P < 0.01. (D) Invasion ability in BxPC3 mock and BxPC3 TFshRNA. BxPC3 mock and BxPC3 TFshRNA diluted in 500 μL of serum-free DMEM were added to the upper wells of a Transwell™ 24-well insert coated with Matrigel®. DMEM supplied with 10% FBS was added to the lower wells. Data are expressed as the mean ± SD. * P < 0.05. The images show the invasion cells. Scale bar 100 μm. (E) Representative fluorescence images of liver, mesentery, and stomach bearing BxPC3 mock GFP or BxPC3 TFshRNA GFP orthotopically. GFP signal denotes the presence of tumour cells. (F) A dissemination score was calculated to evaluate local tumour invasion and distant metastasis as previously described. Data are expressed as the mean ± SD. N = 4–6. ** P < 0.01.**

mock) as a control. BxPC3 TFshRNA appeared to reduce TF expression by 80% at both the mRNA level and protein level (Fig. 1C). BxPC3 TFshRNA showed significant reduction in invasive ability compared with BxPC3 mock in DMEM medium containing 10% FBS (Fig. 1D). We next examined if TF promotes BxPC3 metastasis and invasion in the pancreatic orthotopic tumour xenografts. In the BxPC3 mock orthotopic tumour model, extensive invasion and metastasis was observed in the liver, mesentery and stomach (Fig. 1E). On the other hand, invasion and metastasis was suppressed in the BxPC3 TFshRNA orthotopic tumour model (Fig. 1E). The progression score reflecting tumour invasion and metastasis was significantly decreased in the BxPC3 TFshRNA tumour compared with the BxPC3 mock tumour (Fig 1F).

### 3.2. *TF-VIIa complex induces MMP-9 expression and promotes cancer cell invasion*

To determine a possible TF-mediated invasion factor in the BxPC3 cell line, we examined MMP-2, MMP-7 and MMP-9 expression levels by real-time PCR. Expression of MMP-2 and MMP-7 was very low both in BxPC3 mock and BxPC3 TFshRNA. In contrast, MMP-9 was highly expressed in BxPC3 mock and was significantly reduced in BxPC3 TFshRNA (Fig. 2A). We, therefore, clarified that TF induced MMP-9 production and promoted the invasion ability of pancreatic cancer cells under DMEM containing 10% FBS (Fig. 1). To avoid the effect of factor VIIa in FBS on MMP-9 expression and to determine whether or not the TF-VIIa complex induces MMP-9 followed by promoting

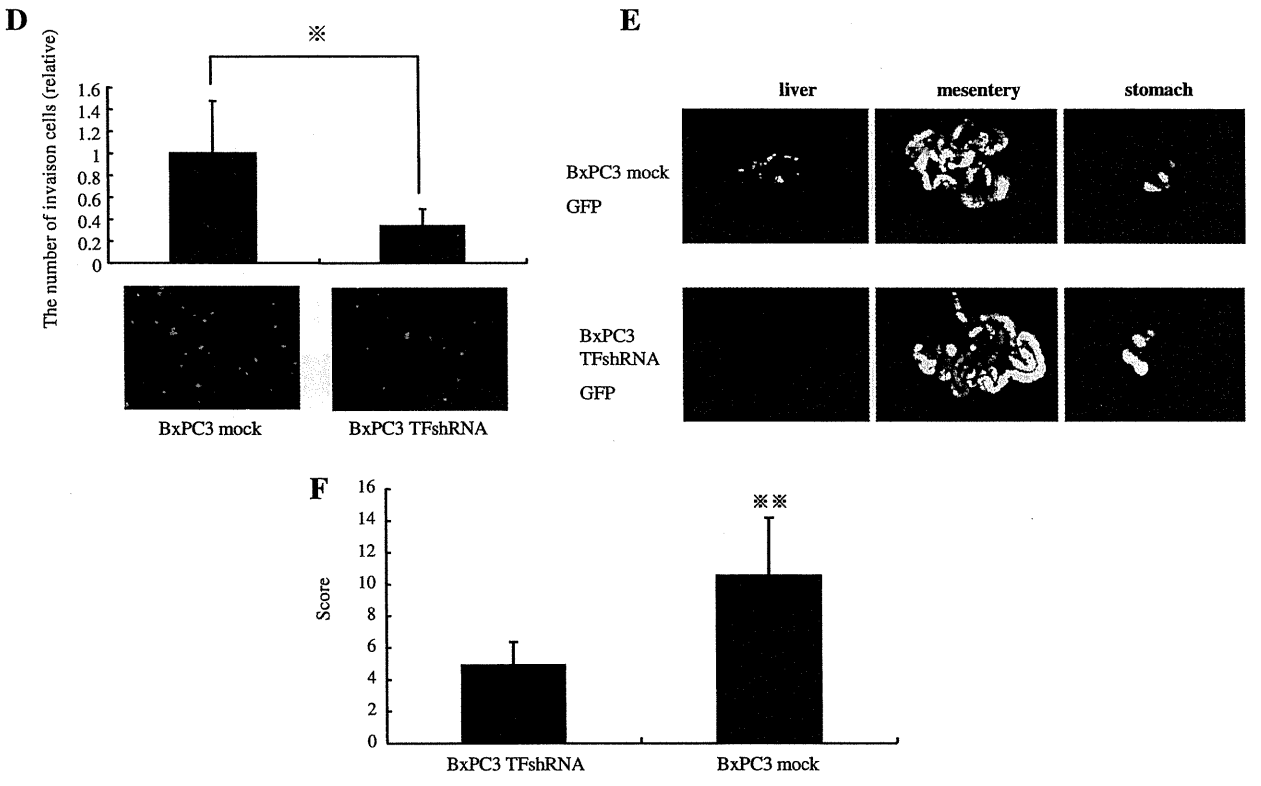


**Fig 1.** (*continued*)

BxPC3 cell invasion, BxPC3 was cultured under FBS-free DMEM (serum starvation). Gelatin zymography showed that BxPC3 mock with factor VIIa significantly increased MMP-9 production compared with BxPC3 mock without factor VIIa (Fig. 2B). However, MMP-9 was not detected in BxPC3 TFshRNA, with or without factor VIIa (Fig. 2B). Invasion assay showed that factor VIIa significantly enhanced the invasion ability of BxPC3 mock but not BxPC3 TFshRNA. This data strongly suggested that the TF-VIIa complex promotes MMP-9 production followed by enhancing cancer cell invasion (Fig. 2C).

### 3.3. *Establishment of neutralisation antibody that inhibits both the blood coagulation cascade and cell signalling of TF*

To establish an anti-human TF neutralisation antibody, we screened 14 hybridoma clones producing rat anti-human TF antibody. The supernatant of hybridoma clones 444 and 1849 significantly inhibited factor X activity (Supplemental Fig. A). Next, we purified the antibody from clones 1849, 72 and 130. The inhibition ability of these clones is strong, modest, and poor, respectively. We next observed whether or not these antibodies inhibit human blood clotting. Antibody 1849 strongly inhibited fibrin clotting in a concentration-dependent manner and prolonged the clotting time to the same level as spontaneous clotting without TF. Antibody 72 modestly inhibited fibrin clotting. In contrast, antibody 130 was unable to inhibit fibrin clotting (Supplemental Fig. B). The same results were obtained using mouse plasma (Supplemental Fig. C). These results suggested that rat anti-human TF antibody purified from hybridoma clone 1849 possessed the most potent TF neutralising effect in terms of blood coagulation cascade. We also determined whether or not antibody 1849 inhibits the TF-VIIa-mediated cell signalling pathway. To determine if 1849 inhibits MMP-9, we examined MMP-9 production by gelatin zymography in BxPC3 mock in the presence of factor VIIa. It was observed that factor VIIa promoted MMP-9 production in BxPC3 mock again (Fig. 2B, Supplemental Fig. D). Interestingly, TF neutralisation antibody 1849 suppressed TF-VIIa-mediated MMP-9 production partly, but the non-specific antibody was unable to suppress production (Supplemental Fig. D). This result showed that antibody 1849 could inhibit not only fibrin clotting but also TF-related cell signalling. Immunocytochemistry with 1849 showed TF in TF-positive cells (Capan1 and BxPC3), whereas there was no detectable TF in TF-negative cells (Panc1 and Mia Paca2) (Supplemental Fig. E). In addition, we confirmed that human TF interacts with mouse factor VIIa, and 1849 inhibits the interaction of human TF and mouse factor VIIa (Supplemental Fig. C), but 1849 does not react with mouse TF (data not shown).

### 3.4. *Inhibitory effect of anti-TF mAb (1849) on cancer cell invasion in vitro*

Since 1849 was able to block both TF-related cell signalling and the blood coagulation function (Supplemental Figures), we predicted that it would inhibit both the promotion of cancer invasion via TF-related cell signalling and haematogenous metastasis via TF-related blood coagulation function. First, we examined the invasion ability in BxPC3 mock in the presence of factor VIIa and/or TF neutralisation antibody

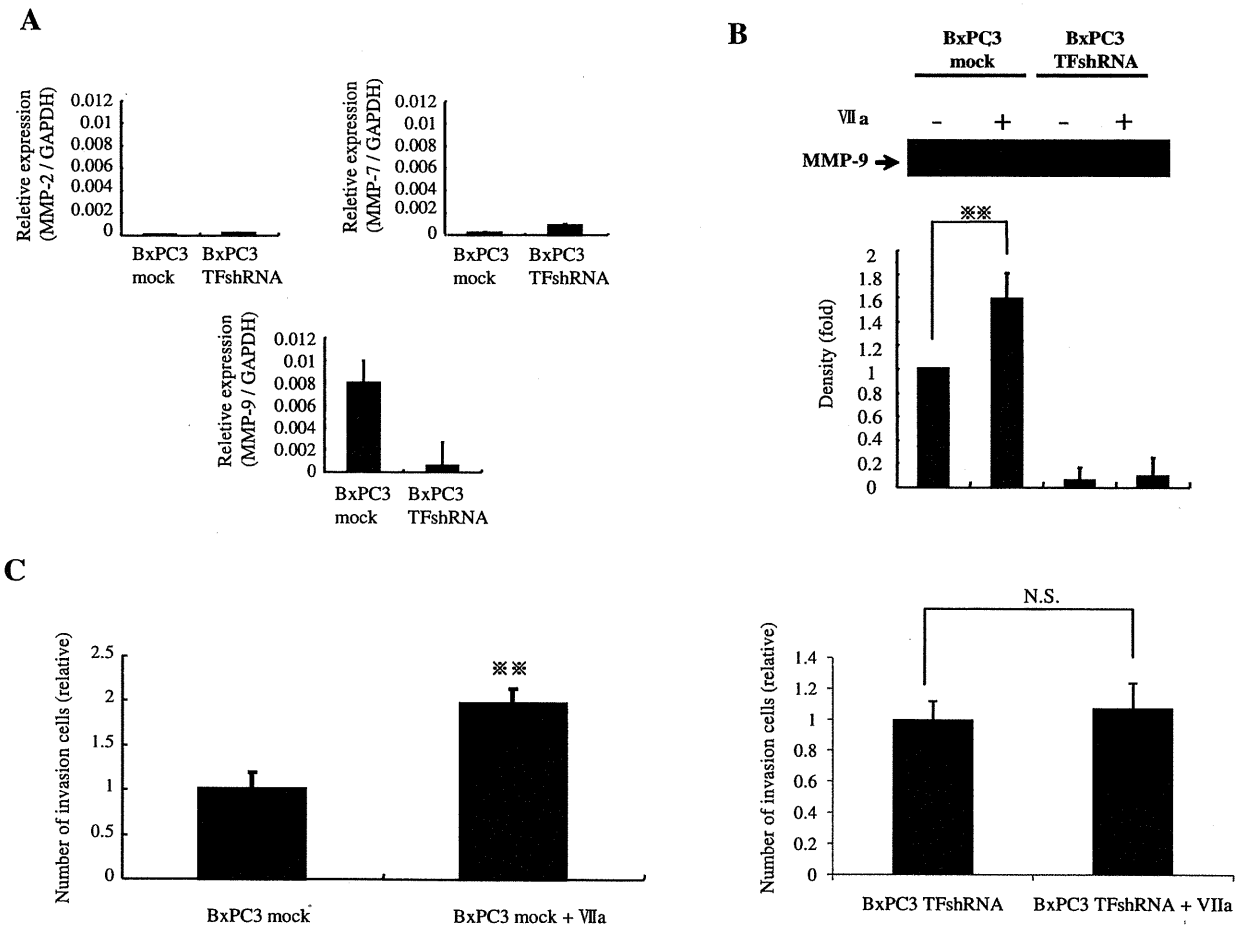


**Fig. 2 – TF-VIIa complex promotes the expression of MMP-9 and invasion. (A) Expression of MMP-2, MMP-7 and MMP-9 by real-time PCR in BxPC3 mock and BxPC3 TFshRNA. Data are expressed as the mean ± SD. (B) Gelatin zymography of culture medium in BxPC3 mock and BxPC3 TFshRNA with or without factor VIIa (5 nM) after starvation for 2 h. MMP-9 was quantified using Image J software. Data are expressed as the mean ± SD. ** $P < 0.01$. (C) Invasion ability in BxPC3 mock or BxPC3 TFshRNA treated with factor VIIa (50 nM). Data are expressed as the mean ± SD. ** $P < 0.01$. N.S. means not significant.**

1849. *In vitro* invasion study showed that the TF neutralisation antibody inhibited the invasion of BxPC3 mock in the presence of factor VIIa compared with the non-specific antibody (Fig. 3A).

### 3.5. *Effect of anti-TF mAb (1849) in mouse model*

In the portal-injection liver metastasis model, cancer cells stayed in the liver and luminescence continued to increase in a time-dependent manner in the control group. On the other hand, in the mice receiving 1849 treatment, luminescence began to decrease from 5 to 10 h after the injection of cancer cells (Fig. 3B). 1849 completely inhibited liver metastasis on Day 4, but the control did not (Fig. 3C). In the orthotopic pancreatic tumour xenograft model, remarkably strong invasion and metastasis were manifested in the liver, mesentery and stomach in the control group (Fig. 4A). In contrast, TF neutralisation antibody 1849 was able to suppress invasion (Fig. 4A). Furthermore, the progression score reflecting invasion and metastasis in the pancreatic orthotopic tumour xenograft was significantly lower in the 1849-treatment group compared with that in the control group (Fig. 4B). In addition, cancer spreading beyond the pancreas was observed in the control group. On the other hand, pancreatic cancer cells remained within the pancreas even after 6 weeks of injection of cancer cells in the 1849-treatment group (Fig. 4C). Kaplan–Meier analysis showed a significant improvement in survival rate in the 1849 treatment group compared to the control group (Fig. 4D). A significant difference in body change between the 1849-treatment mice and the control mice was not observed (Fig. 4E).

## 4. Discussion

Pancreatic cancer is the most refractory neoplasm and possesses several clinicopathological characteristics. First, pancreatic cancer exerts extensive invasion and metastasis to other organs.[14,15] Second, thrombosis occurs most frequently in patients with pancreatic cancer.[7] Third, expression of TF may contribute to the aggressiveness of pancreatic cancer that stimulates tumour invasiveness, and evaluation of the primary tumour for TF expression may identify patients with a poor prognosis.[17,18] We, therefore, hypothesised that TF

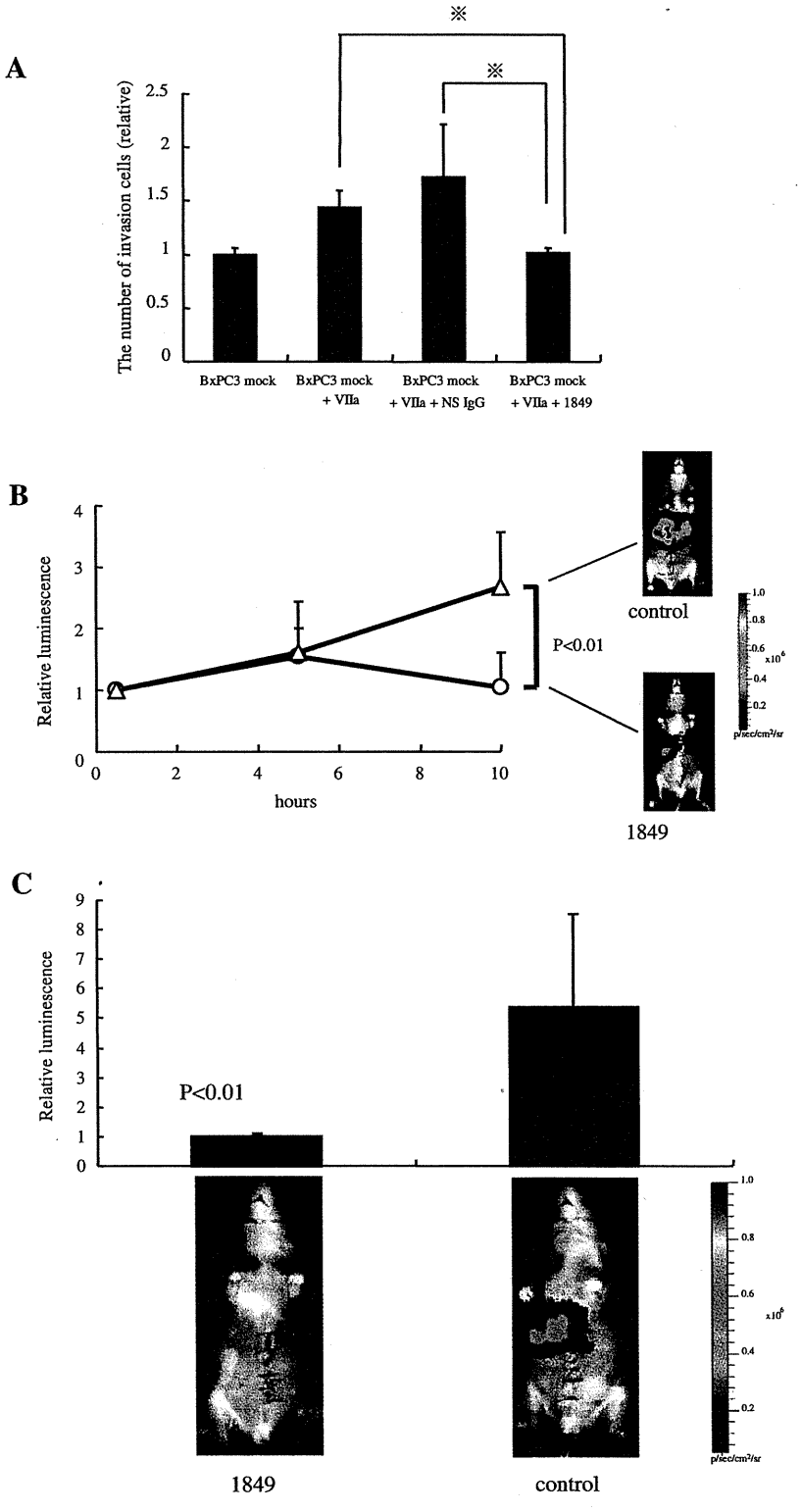


**Fig. 3 – Anti-human neutralisation antibody 1849 inhibits cancer cell invasion and haematogenous metastasis. (A) Invasion ability in BxPC3 mock treated with factor VIIa (50 nM) clone 1849 (100 μg/ml), or non-specific antibody (anti-human CD20 antibody, 100 μg/ml). Data are expressed as the mean ± SD. * $P < 0.05$. (B) Inhibition of early-phase metastasis by 1849 in portal-injection liver metastasis model. Luminescence intensity was measured by IVIS imaging system 0, 5, and 10 h after injection of cancer cells. Data are expressed as the mean ± SD. N = 6. (C) Inhibition of late-phase metastasis by 1849. Luminescence intensity was measured by IVIS imaging system 4 days after injection of cancer cells. Data are expressed as the mean ± SD. N = 5.**

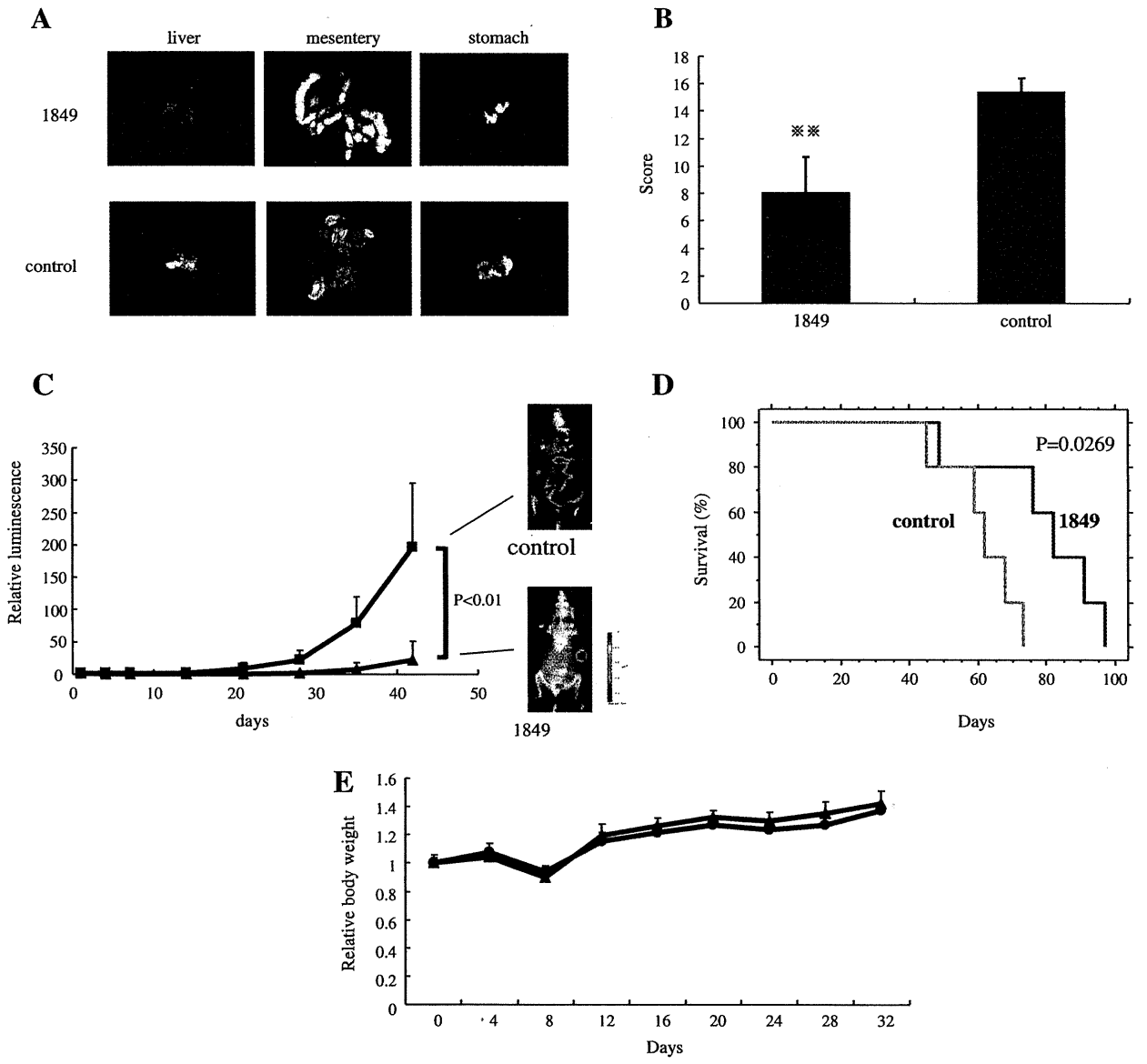


**Fig. 4 – The effect of 1849 in the mouse model. (A) Representative fluorescence images of liver, mesentery and stomach bearing BxPC3 mock GFP treated with 1849 or PBS. GFP signal denotes the presence of tumour cells. (B) A dissemination score was calculated to evaluate local tumour invasion and distant metastasis as previously described. Data are expressed as the mean ± SD. N = 5–6. ** P < 0.01. (C) Inhibition of invasion and metastasis by 1849 in pancreatic orthotopic tumour xenografts. Relative luminescence was quantitated by IVIS imaging system. Representative luminescence intensity images were obtained in the individual control and the 1849-treated group. Data are expressed as the mean ± SD. N = 5. D. Effect of 1849 treatment on survival. Survival was assessed by Kaplan–Meier analysis. Blue line represents the 1849 treatment group. Green line indicates the control group. N = 5. E. Body weight change by 1849. Mice inoculated with BxPC3 cells subcutaneously on Day 0 were treated for seven consecutive days with 1849 mAb (400 μg/mouse, ●) as the TF neutralisation antibody, or PBS (▲) as the control. N = 3.**

plays an important role in the invasion-metastasis cascade of pancreatic cancer.

In this study, the expression pattern of TF in BxPC3, TF-abundant cancer cells, was different between *in vitro* and *in vivo*. These results corresponded with a previous study on the human squamous cell carcinoma cell line A431.[21] Both A431 and BxPC3 are uniformly expressed *in vitro*. A431 xenografts were heterogeneously stained for TF; however, our study showed BxPC3 xenografts highly expressed in the area of cancer cells contacting with stromal cells, namely the invasion front. In fact, invasion assay showed that BxPC3 TFshRNA cell lines strongly inhibited cell invasion compared with BxPC3 mock cell lines. Real-time PCR analysis showed that the expression of MMP-9 in the BxPC3 TFshRNA cell line decreased compared with BxPC3 mock. To date, many reports have shown that MMP-9 promotes the invasion of pancreatic cancer.[3,22] In BxPC3, the invasion ability was suppressed through the inhibition of MMP-9 expression by SiRNA.[23]

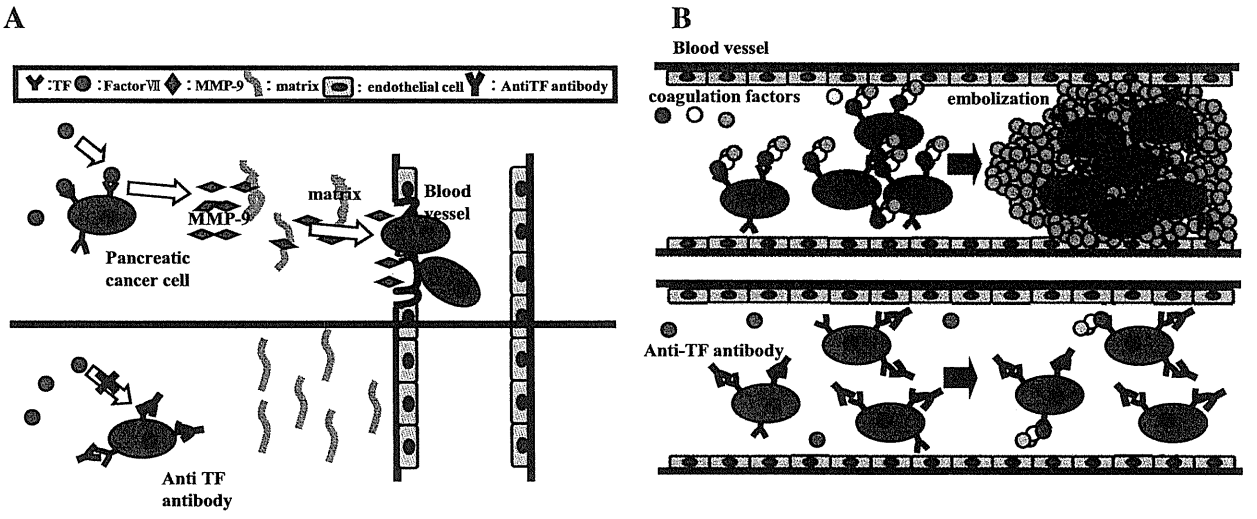


**Fig. 5 – Possible role of TF-VIIa complex on invasion and metastasis. And the implication of anti-human TF neutralisation antibody, 1849, against the tumour metastasis. (A) TF-VIIa in pancreatic cancer induces MMP-9 expression and invades stromal tissue and basement membrane. 1849 inhibits invasion by inhibiting TF-related cell signalling. (B) TF-VIIa promotes embolisation in micro blood vessels. 1849 inhibits blood coagulation and traps cancer cells.**

Taking our present data and other reports together, TF promotes the invasion ability of BxPC3 by expressing MMP-9.

Previous reports showed the relationship between coagulation factors and MMPs. In normal tissue, PAR-2, which is downstream from TF-VIIa complex signalling, mediates MMP-9 release in airway epithelial cells.[24] Thrombin mediates an increase in MMP-1 and MMP-3 in human endothelial cells.[25] In cancer tissue, PARs mediate MMP-2 and MMP-9 in prostate cancer.[26] Also, in colorectal adenocarcinoma cells, the TF-VIIa complex induces the expression of MMP-7.[27] However, in pancreatic cancer cells, the relationship between coagulation factor(s) and MMP(s) remains unclear. Our study is the first evidence that the TF-VIIa complex induces MMP-9 and promotes invasion in pancreatic cancer cells. Moreover, we also showed that TF promoted invasion *in vivo* using pancreatic orthotopic tumour xenografts.

Next, we newly established a TF neutralisation antibody for the treatment of pancreatic cancer. We found that the anti-TF antibody 1849 decreased the release of MMP-9. Therefore, we propose that 1849 inhibits TF-related cell signalling by blocking the TF-VIIa complex. Also, blood coagulation assay showed that 1849 inhibited TF-induced blood coagulation to the same level as the TF-free sample. We suggest from this result that 1849 can almost completely inhibit TF-related blood coagulation.

We found that 1849 inhibited pancreatic cancer invasion in the *in vitro* invasion assay. We suggest that this anti-invasion effect of 1849 is due to MMP-9 suppression via TF-related cell signalling. Also, 1849 completely blocked haematogenous metastasis in the portal-injection liver metastasis mouse model. This result suggested that the anti-haematogenous metastasis effect of 1849 is due to blocking the TF-related blood coagulation cascade.

Since the metastatic ability of BxPC3 TFshRNA decreased significantly as compared to that of BxPC3 mock *in vivo*, we tested if our newly developed anti- TF mAb suppressed the metastasis of BxPC3. We used the orthotopic pancreatic tumour xenograft model to examine whether or not 1849 could block invasion and metastasis in the mouse model, because the orthotopic model is similar to human pancreatic cancer in terms of progression, invasion, and metastasis.[19] 1849 strongly inhibited invasion and metastasis. Moreover, the survival rate in the 1849 treatment group was significantly improved compared with that of the control group.

The metastasis process includes many steps. Cancer cells invade the basement membrane and the pericytes of blood vessels. Cancer cells survive in the bloodstream and end up in the micro blood vessels of distant organs. MMP-9 plays an important role in invasion. Fibrin facilitates metastasis by enhancing the sustained adherence and survival of tumour cell emboli in the blood vessels of distant organs.[10] Also, a recent study showed that fibrin increases the metastatic potential of circulating tumour cells by impeding natural killer cells.[28] 1849 almost completely inhibited both blood coagulation and TF-VIIa complex mediated MMP-9 release.

In summary, we found that the TF-VIIa complex upregulated MMP-9 and promoted cancer invasion in pancreatic cancer. The cancer cells subsequently degraded the stromal extracellular matrix and basement membrane to intravasate into the blood vessels (Fig. 5A). Next, they formed microthrombi within the vessels (Fig. 5B). The double-blocking effect of our newly developed TF neutralisation antibody 1849 could be a useful tool in the treatment of pancreatic cancer invasion-metastasis.

## Grant support

This work was supported partly by a Grant-in-Aid from the Third Term Comprehensive Control Research for Cancer, the Ministry of Health, Labor and Welfare (Matsumura, H19-025), Scientific Research on Priority Areas from the Ministry of Education, Culture, Sports, Science and Technology

(Matsumura, 17016087), and the Japanese Foundation for Multidisciplinary Treatment of Cancer (Matsumura), Funding Program for World-Leading Innovative R&D on Science and Technology (FIRST Program) and the Princess Takamatsu Cancer Research Fund (07-23908). Yohei Saito was supported by Research Fellowships from the Japan Society for the Promotion of Science for Young Scientists.

## Conflict of interest statement

None declared.

## Acknowledgements

We thank Dr. Miyawaki (RIKEN) for Venus. We thank N. Mie and M. Ohtsu for their technical assistance, and K. Shiina for her secretarial assistance.

## Appendix A. Supplementary data

Supplementary data associated with this article can be found, in the online version, at doi:10.1016/j.ejca.2011.04.028.

REFERENCES

1. Fidler IJ. The pathogenesis of cancer metastasis: the 'seed and soil' hypothesis revisited. *Nat Rev Cancer* 2003;**3**:453–8.
2. Curran S, Murray GI. Matrix metalloproteinases: molecular aspects of their roles in tumour invasion and metastasis. *Eur J Cancer* 2000;**36**:1621–30.
3. Nagakawa Y, Aoki T, Kasuya K, Tsuchida A, Koyanagi Y. Histologic features of venous invasion, expression of vascular endothelial growth factor and matrix metalloproteinase-2 and matrix metalloproteinase-9, and the relation with liver metastasis in pancreatic cancer. *Pancreas* 2002;**24**:169–78.
4. Edgington TS, Mackman N, Brand K, Ruf W. The structural biology of expression and function of tissue factor. *Thromb Haemost* 1991;**66**:67–79.
5. Ruf W, Edgington TS. Structural biology of tissue factor, the initiator of thrombogenesis *in vivo*. *FASEB J* 1994;**8**:385–90.
6. Varki A. Trousseau's syndrome: multiple definitions and multiple mechanisms. *Blood* 2007;**110**:1723–9.
7. Stein PD, Beemath A, Meyers FA, et al. Incidence of venous thromboembolism in patients hospitalized with cancer. *Am J Med* 2006;**119**:60–8.
8. Belting M, Ahamed J, Ruf W. Signaling of the tissue factor coagulation pathway in angiogenesis and cancer. *Arterioscler Thromb Vasc Biol* 2005;**25**:1545–50.
9. Sampson MT, Kakkar AK. Coagulation proteases and human cancer. *Biochem Soc Trans* 2002;**30**:201–7.
10. Palumbo JS, Kombrinck KW, Drew AF, et al. Fibrinogen is an important determinant of the metastatic potential of circulating tumor cells. *Blood* 2000;**96**:3302–9.
11. Morris DR, Ding Y, Ricks TK, et al. Protease-activated receptor-2 is essential for factor VIIa and Xa-induced signaling, migration, and invasion of breast cancer cells. *Cancer Res* 2006;**66**:307–14.
12. Hjortoe GM, Petersen LC, Albrektsen T, et al. Tissue factor-factor VIIa-specific up-regulation of IL-8 expression in MDA-MB-231 cells is mediated by PAR-2 and results in increased cell migration. *Blood* 2004;**103**:3029–37.
13. Jemal A, Siegel R, Ward E, et al. Cancer statistics, 2008. *CA Cancer J Clin* 2008;**58**:71–96.
14. Warshaw AL, Fernández-del Castillo C. Pancreatic carcinoma. *N Engl J Med* 1992;**326**:455–65.
15. Wanebo HJ, Vezeridis MP. Pancreatic carcinoma in perspective. A continuing challenge. *Cancer* 1996;**78**:580–91.
16. Khorana AA, Ahrendt SA, Ryan CK, et al. Tissue factor expression, angiogenesis, and thrombosis in pancreatic cancer. *Clin Cancer Res* 2007;**13**:2870–5.
17. Kakkar AK, Lemoine NR, Scully MF, Tebbutt S, Williamson RC. Tissue factor expression correlates with histological grade in human pancreatic cancer. *Br J Surg* 1995;**82**:1101–4.
18. Nitori N, Ino Y, Nakanishi Y, et al. Prognostic significance of tissue factor in pancreatic ductal adenocarcinoma. *Clin Cancer Res* 2005;**11**:2531–9.
19. Saito Y, Yasunaga M, Kuroda J, Koga Y, Matsumura Y. Antitumour activity of NK012, SN-38-incorporating polymeric micelles, in hypovascular orthotopic pancreatic tumour. *Eur J Cancer* 2010;**46**:650–8.
20. Hotz HG, Reber HA, Hotz B, et al. An orthotopic nude mouse model for evaluating pathophysiology and therapy of pancreatic cancer. *Pancreas* 2003;**26**:e89–98.
21. Milsom CC, Yu JL, Mackman N, et al. Tissue factor regulation by epidermal growth factor receptor and epithelial-to-mesenchymal transitions: effect on tumor initiation and angiogenesis. *Cancer Res* 2008;**68**:10068–76.
22. Määttä M, Soini Y, Liakka A, Autio-Harmainen H. Differential expression of matrix metalloproteinase (MMP)-2, MMP-9, and membrane type 1-MMP in hepatocellular and pancreatic adenocarcinoma: implications for tumor progression and clinical prognosis. *Clin Cancer Res* 2000;**6**:2726–34.
23. Wang Z, Banerjee S, Li Y, et al. Down-regulation of notch-1 inhibits invasion by inactivation of nuclear factor-kappaB, vascular endothelial growth factor, and matrix metalloproteinase-9 in pancreatic cancer cells. *Cancer Res* 2006;**66**:2778–84.
24. Vliagoftis H, Schwingshackl A, Milne CD, et al. Proteinase-activated receptor-2-mediated matrix metalloproteinase-9 release from airway epithelial cells. *J Allergy Clin Immunol* 2000;**106**:537–45.
25. Duhamel-Clérin E, Orvain C, Lanza F, Cazenave JP, Klein-Soyer C. Thrombin receptor-mediated increase of two matrix metalloproteinases, MMP-1 and MMP-3, in human endothelial cells. *Arterioscler Thromb Vasc Biol* 1997;**17**:1931–8.
26. Wilson SR, Gallagher S, Warpeha K, Hawthorne SJ. Amplification of MMP-2 and MMP-9 production by prostate cancer cell lines via activation of protease-activated receptors. *Prostate* 2004;**60**:168–74.
27. Zhang JQ, Wan YL, Liu YC, et al. The FVIIa-tissue factor complex induces the expression of MMP7 in LOVO cells *in vitro*. *Int J Colorectal Dis* 2008;**23**:971–8.
28. Palumbo JS, Talmage KE, Massari JV, et al. Platelets and fibrin(ogen) increase metastatic potential by impeding natural killer cell-mediated elimination of tumor cells. *Blood* 2005;**105**:178–85.

Journal of Controlled Release xxx (2012) xxx–xxx

Contents lists available at SciVerse ScienceDirect

Journal of Controlled Release

journal homepage: www.elsevier.com/locate/jconrel

# Polymeric micelles incorporating (1,2-diaminocyclohexane)platinum (II) suppress the growth of orthotopic scirrhous gastric tumors and their lymph node metastasis

Md. Rafi [a], H. Cabral [b], M.R. Kano [c,f], P. Mi [b], C. Iwata [c], M. Yashiro [d], K. Hirakawa [d], K. Miyazono [c,f], N. Nishiyama [a,f,*], K. Kataoka [a,b,e,f,**]

[a] Center for Disease Biology and Integrative Medicine, Graduate School of Medicine, The University of Tokyo, 7-3-1 Hongo, Bunkyo-ku, Tokyo 113-0033, Japan
[b] Department of Bioengineering, Graduate School of Engineering, The University of Tokyo, 7-3-1 Hongo, Bunkyo-ku, Tokyo, 113-8656, Japan
[c] Department of Molecular Pathology, Graduate School of Medicine, The University of Tokyo, 7-3-1 Hongo, Bunkyo-ku, Tokyo 113-0033, Japan.
[d] Department of Surgical Oncology, Medical School, Osaka City University, Osaka, Japan
[e] Department of Materials Engineering, Graduate School of Engineering, The University of Tokyo, 7-3-1 Hongo, Bunkyo-ku, Tokyo 113-8656, Japan
[f] Center for NanoBio Integration, The University of Tokyo, 7-3-1 Hongo, Bunkyo-ku, Tokyo 113-8656, Japan

ARTICLE INFO

*Article history:*
Received 24 October 2011
Accepted 27 January 2012
Available online xxxx

*Keywords:*
Drug delivery
Chemotherapy
Polymeric micelles
Gastric cancer
Lymph node metastasis

ABSTRACT

Nano-scaled drug carriers have great potential for the treatment of solid tumors. Nevertheless, hypovascularity and fibrosis in some types of solid tumors have been demonstrated to reduce the penetration and accumulation of nano-scaled drug carriers. Diffuse-type scirrhous gastric cancers present such characteristics as well as frequent metastasis to the lymph nodes; therefore, it remains a great challenge to eradicate scirrhous gastric cancers based on the drug targeting using nanocarriers. Herein, we demonstrated that polymeric micelles with 30-nm diameter incorporating (1,2-diaminocyclohexane)platinum(II) (DACHPt), the parent complex of the anticancer drug oxaliplatin, efficiently penetrated and accumulated in an orthotopic scirrhous gastric cancer model, leading to the inhibition of the tumor growth. Moreover, the elevated localization of systemically injected DACHPt-loaded micelles in metastastic lymph nodes reduced the metastatic tumor growth. These results suggest DACHPt-loaded micelles as a promising nanocarrier for the treatment of scirrhous gastric cancers and their lymphatic metastases.



## 1. Introduction

Nano-scaled drug carriers are being developed for improving the treatment of solid tumors while decreasing the toxicity [1–5]. These nanocarriers effectively accumulate in solid tumors due to the hyperpermeability of blood capillaries to circulating macromolecules and the impaired lymphatic drainage of these macromolecules, which are known as the Enhanced Permeability and Retention (EPR) effect [6]. Indeed, several nanocarrier formulations have been approved for clinical use against hypervascular cancers such as ovarian cancers, HIV-associated Kaposi's sarcoma and breast cancers [7,8]. However, in some intractable cancers such as pancreatic and gastric cancers, the hypovascularity and fibrosis of tumors may compromise the extravasation and tissue penetration of nanocarriers [9,10].

Gastric cancers cause 1 million deaths per year worldwide being the 2nd leading cause of cancer-related death following lung cancer [11]. Among gastric cancers, a diffuse-type scirrhous gastric cancer (SGC) affects younger patients and presents the highest mortality [12]. SGC is characterized by hypovascularity, extensive stromal fibrosis and metastasis to the lymph nodes [13–15]. These characteristics impair the therapeutic efficacy of chemotherapy as well as nanocarrier-mediated targeting chemotherapy. Moreover, the targeting chemotherapy against lymph node metastasis involve intralymphatic or local administration of nanocarrier-encapsulated antitumor agents [16–18]; however, these approaches may not target all draining lymph nodes due to the inappropriate position of the injection [18] and the obstruction of lymphatic vessels in advanced stages of cancer [18–19]. Hence, the improved targeting against the lymph node metastasis is strongly needed to eradicate the lymph node metastasis.

Polymeric micelles, self-assemblies of block copolymers are characterized by the core-shell structures with drug-loaded core surrounded by hydrophilic PEG shell, and have shown great potential as tumor-targetable nanocarriers [3–5]. The substantial advantages of polymeric micelles include relatively small size ranging from 20 to 100 nm, controllable drug loading and release, and favorable biodistribution including prolonged blood circulation and enhanced tumor accumulation [3–5]. Accordingly, micelle formulations

* Correspondence to: N. Nishiyama, Center for Disease Biology and Integrative Medicine, Graduate School of Medicine, The University of Tokyo, 7-3-1 Hongo, Bunkyo-ku, Tokyo 113-0033, Japan. Tel.: +81 3 5841 1430; fax: +81 3 5841 1419.
** Correspondence to: K. Kataoka, Department of Materials Engineering, Graduate School of Engineering, The University of Tokyo, 7-3-1 Hongo, Bunkyo-ku, Tokyo 113-8656, Japan. Tel.: +81 3 5841 7138; fax: +81 3 5841 7139.
*E-mail addresses:* nishiyama@bmw.t.u-tokyo.ac.jp (N. Nishiyama), kataoka@bmw.t.u-tokyo.ac.jp (K. Kataoka).

0168-3659/$ – see front matter © 2012 Elsevier B.V. All rights reserved.
doi:10.1016/j.jconrel.2012.01.038

incorporating doxorubicin, SN-38, paclitaxel, cisplatin, and (1,2-diaminocyclohexane)platinum(II) (DACHPt) (an active form of oxaliplatin) exerted significant efficacy against several tumor models with appreciably lowered toxicity compared to free drugs, and are currently under clinical evaluation [20–24]. Particularly, DACHPt-loaded polymeric micelles (DACHPt/m) are characterized by the small size (ca. 30 nm) [25–26], achieving high penetration into tumor mass and remarkable antitumor activity against poorly permeable tumors such as pancreatic tumors [27–29].

This study was aimed to evaluate the targeting ability and therapeutic efficiency of systemically injected DACHPt/m against a well-established experimental model of SGC, which was prepared by orthotopic inoculation of OCUM-2MLN scirrhous gastric cancer cells [30–31]. In the orthotopic SGC model of OCUM-2MLN cells, the induction of lymph node metastasis occurs in all mice, while the tumor microenvironment shows hypovascularity and thick fibrosis similar to SGC in the patients, indicating the clinical relevancy of this model [30–31]. Here, the therapeutic potential of the DACHPt/m against orthotopic SGC and their lymph node metastasis was examined by using bioluminescent OCUM-2MLN-Luc tumors.

## 2. Materials and methods

### 2.1. Materials

Bis(trichloromethyl)carbonate (triphosgene) was purchased from Tokyo Kasei Kogyo Co., Inc. (Tokyo, Japan). γ-Benzyl L-glutamate was purchased from Sigma Chemical Co., Inc. (St. Louis, MO). *N,N*-Dimethylformamide (DMF) and 3-(4,5-dimethylthiazol-2-yl)-2,5-diphenyltetrazolium bromide (MTT) were obtained from Wako Pure Chemical Co., Inc. (Osaka, Japan). Dichloro(1,2-diamminocyclohexane) platinum(II) ($DACHPtCl_2$) was purchased from Heraeus (Germany). $AgNO_3$ was purchased from Aldrich Chemical Co., Inc. (Milwaukee, WI). α-Methoxy-ω-amino poly(ethylene glycol) ($CH_3O$-PEG-$NH_2$; Mw = 12,000) was purchased from NOF Co., Inc. (Tokyo, Japan). Alexa 594- and Alexa 680-*N*-hydroxysuccinimide ester were purchased from Invitrogen (USA).

### 2.2. Animals and cells

Immunodeficient BALB/c nu/nu mice at 6 weeks of age were obtained from Charles River Laboratories (Tokyo, Japan), and treated in accordance with the policies of the Animal Ethics Committee of The University of Tokyo. Human diffuse-type gastric carcinoma OCUM-2MLN cells were used for the model of diffuse-type scirrhous gastric cancer (SGC) with high frequency of the lymph node metastasis [30–31]. OCUM-2MLN cells were maintained in Dulbecco's Modified Eagle Media (DMEM) (Sigma Chemicals) supplemented with 10% fetal bovine serum (FBS) in a humidified atmosphere containing 5% $CO_2$ at 37 °C.

### 2.3. Preparation of PEG-b-P(Glu)

Poly(ethylene glycol)-poly(L-glutamic acid) block copolymers (PEG-*b*-P(Glu)) were synthesized according to the previously described synthetic method with a slight modification [25]. Briefly, *N*-carboxy anhydride of γ-benzyl L-glutamate was polymerized in DMF, initiated by the primary amino group of $CH_3O$-PEG-$NH_2$ to obtain PEG-poly(γ-benzyl-L-glutamate) block copolymer (PEG-*b*-PBLG). A narrow distribution (Mw/Mn: 1.06) of PEG-*b*-PBLG was confirmed by gel permeation chromatography [column: TSK-gel G3000HHR, G4000HHR (Tosoh, Yamaguchi, Japan); eluent: DMF containing 10 mM LiCl; flow rate: 0.8 ml/min; detector: refractive index (RI); temperature: 25 °C]. The polymerization degree of PBLG was determined to be 20 by comparing the proton ratios of methylene units in PEG (—$OCH_2CH_2$—: δ = 3.7 ppm) and phenyl groups of PBLG (—$CH_2C_6H_5$—: δ = 7.3 ppm) in $^1$H-NMR measurement [JEOL EX270 (JEOL, Tokyo, Japan); solvent: DMSO-$d_6$; temperature: 80 °C]. The deprotection of the benzyl group of PEG-*b*-PBLG was carried out by mixing with 0.5 N NaOH at room temperature to obtain PEG-*b*-P(Glu).

PEG-*b*-P(Glu) was fluorescent-labeled by the conjugation of Alexa 594- or Alexa 680-succinimidyl esters to the ω-amino group of the polymer in DMSO. Twenty-four hours later, the polymers were purified by dialysis against DMSO followed by water. Finally, the solutions were freeze-dried, and the amount of conjugated dye was determined to be approximately 70% (% fluorescent dye / PEG-*b*-P(Glu)) by fluorescence spectroscopy.

### 2.4. Preparation of DACHPt-loaded micelles (DACHPt/m)

DACHPt/m were prepared according to a previously described method [25]. Briefly, $DACHPtCl_2$ (5 mM) was suspended in distilled water and mixed with silver nitrate [$(AgNO_3)$/(DACHPt) = 1] to form $DACHPtCl(NO_3)$. The solution was kept in the dark for 24 h at 25 °C. AgCl precipitate after reaction was eliminated by centrifugation. The supernatant was purified by passage through a 0.22 μm filter. Then, PEG-*b*-P(Glu) [(Glu) = 5 mmol/l] was added to the DACHPt solution [(DACHPt)/(Glu) = 1.0] and reacted for 120 h to prepare DACHPt/m. The prepared micelles were purified by ultrafiltration [molecular weight cutoff size (MWCO): 30,000]. The size distribution of DACHPt/m was evaluated by dynamic light scattering (DLS) measurement at 25 °C, using the Zetasizer Nano ZS90 (Malvern Instruments Ltd., Worcestershire, United Kingdom).

The Pt content of the micelles was determined by using an ion coupled plasma-mass spectrometer (4500 ICP-MS; Hewlett Packard, Palo Alto, CA). Fluorescent-labeled DACHPt/m were prepared in a similar manner with Alexa 594- or Alexa 680-labeled PEG-P(Glu).

#### 2.4.1. In vitro cytotoxicity assay

To determine the cytotoxicity, OCUM-2MLN cells were seeded in a 96 well plate and incubated at 37 °C. Then, the cells were exposed to free oxaliplatin or DACHPt/m for 48 or 72 h, followed by the addition of MTT solution. Cell viability was measured by the formed formazan absorbance at 570 nm.

### 2.5. Preparation of orthotopic SGC models with lymphatic metastasis

Lentiviral vector [32] was used to express the luciferase protein gene stably in OCUM-2MLN cells. The prepared OCUM-2MLN-Luc cells were grown in DMEM containing 10% FBS. For preparation of orthotopic SGC models, OCUM-2MLN-Luc cells were inoculated by orthotopic implantation method. Briefly, after the abdomen of BALB/c nu/nu mice was sterilized with alcohol, an incision was made to expose the stomach, and OCUM-2MLN-Luc cell suspension was injected sub-serosally into the gastric walls as previously described [33]. The stomach was then returned into the peritoneal cavity, and the abdominal wall and the skin were closed with surgical suture.

### 2.6. Evaluation of antitumor activity by bioluminescent imaging

Bioluminescent imaging [34] was carried out with a highly sensitive CCD camera using IVIS imaging system (IVIS, Caliper Life Science, Hopkinton, MA). Imaging and quantification of signals were analyzed by Living Image software (Caliper Life Science). For *in vitro* imaging, bioluminescent cells were diluted in cell culture media in a black, 96-well plate (Costar, Corning, NY). VivoGlo luciferin (Promega, Madison, WI) at 150 μg/ml in media was added to each well 5 min prior to imaging. Imaging was performed for 1 min per plate. For the analysis of antitumor activity, BALB/c nu/nu ($n = 5$) mice were inoculated by orthotopic injection of OCUM-2MLN –Luc cells ($5 \times 10^6$). Tumors were allowed to grow for 3 weeks, to initiate the metastasis to the lymph nodes. Subsequently, the mice received three i.v. injections of oxaliplatin (8 mg/kg)

Please cite this article as: M. Rafi, et al., Polymeric micelles incorporating (1,2-diaminocyclohexane)platinum (II) suppress the growth of orthotopic scirrhous gastric tumors ..., J. Control. Release (2012), doi:10.1016/j.jconrel.2012.01.038

and DACHPt/m (4 mg/kg on a Pt base) on days 0, 2 and 4. Photon flux was measured until 2 weeks and was taken as a parameter of tumor volume. Body weight was measured simultaneously to assess the toxicity.

### 2.7. Antitumor activity against lymph node metastasis

To study the antitumor efficacy of the DACHPt/m against lymphatic metastasis, the mice were sacrificed at the end of the antitumor activity experiment and the metastatic lymph nodes were excised and weighed. The inhibition of the growth of the metastases was associated with the weight of the lymph nodes.

### 2.8. Accumulation of DACHPt/m in orthotopic tumors and metastatic lymph nodes

In order to analyze the biodistribution of oxaliplatin and DACHPt/m, OCUM-2MLN-Luc cells ($5\times10^6$ cells/ml) were injected sub-serosally into the gastric walls of BALB/c nu/nu mice (female, $n=5$). Four weeks later, oxaliplatin and DACHPt/m were intravenously injected at a dose of 100 μg/mouse on a platinum basis. Mice were sacrificed after defined time periods (1, 4 and 24 h), and then tumor and metastatic lymph nodes were collected. Tissue samples were washed in ice-cold saline and weighed after removing excess fluid. All samples were dissolved in $HNO_3$ and evaporated to dryness. The Pt concentration was measured by ICP-MS after the samples were redissolved in 5N HCl.

### 2.9. Biodistribution of fluorescent-labeled DACHPt/m

DACHPt/m were labeled with Alexa 680 to investigate the accumulation in orthotopic gastric tumors and metastatic lymph nodes. OCUM-2MLN ($5\times10^6$ cells/ml) cells were inoculated sub-serosally into the gastric walls of BALB/c nu/nu mice and the tumors were allowed to grow for about 3 weeks. Alexa 680-labeled DACHPt/m (5 mg/kg on Pt basis) were intravenously injected and the mice were imaged after 24 h to track the accumulation of micelles in the whole body by using IVIS imaging system (excitation: 640 nm; emission: 720 nm; exposure time: 1 s; field of view: 18.1 cm). Then, the mice were sacrificed and the organs (liver, kidney and spleen), the primary tumor and the metastatic lymph nodes were imaged *ex vivo* to evaluate the accumulation of micelles.

### 2.10. Microdistribution of fluorescent micelles in orthotopic tumor and lymph node metastasis

Tumor bearing mice were injected intravenously with Alexa 594-labeled DACHPt/m to evaluate their microdistribution in primary tumors and metastatic lymph nodes by histology. Tumors, metastatic and normal lymph nodes were excised, snapped frozen in liquid nitrogen and embedded in optimal cutting temperature compound (Tissue-Tek, Sakura Finetek). The frozen samples were sectioned at 10-μm thickness in a cryostat and fixed with 10% formalin. The tissue sections were stained with hematoxylin and eosin (H&E) and observed using an Olympus AX80 microscope (Olympus, Japan). For immunohistochemical analysis, the tissue sections were also stained for lymphatic vessels by using anti-LYVE-1 antibody (Abcam), blood vessels by using anti-PECAM-1 antibody (BD PharMingen), and cancer cells by using anti-CD326 antibody (EpCAM, Miltenyi biotec), followed by staining with Alexa488- and Alexa647-conjugated secondary antibodies (Invitrogen). Hoechst 33342 was used for nuclear staining. The stained tissue samples were observed using a LSM510 META laser confocal microscope (Carl Zeiss, Germany).

## 3. Results

### 3.1. In vitro characterization of DACHPt-loaded micelles (DACHPt/m)

The polymer-metal complex formation between DACHPt and the carboxylic group of the P(Glu) in the PEG-*b*-P(Glu) led to the formation of polymeric micelles with an average diameters of approximately 30-nm (Fig. 1 and Supplementary Fig. S1A). DACHPt/m can release cytotoxic DACHPt complexes from the micelle core by the ligand

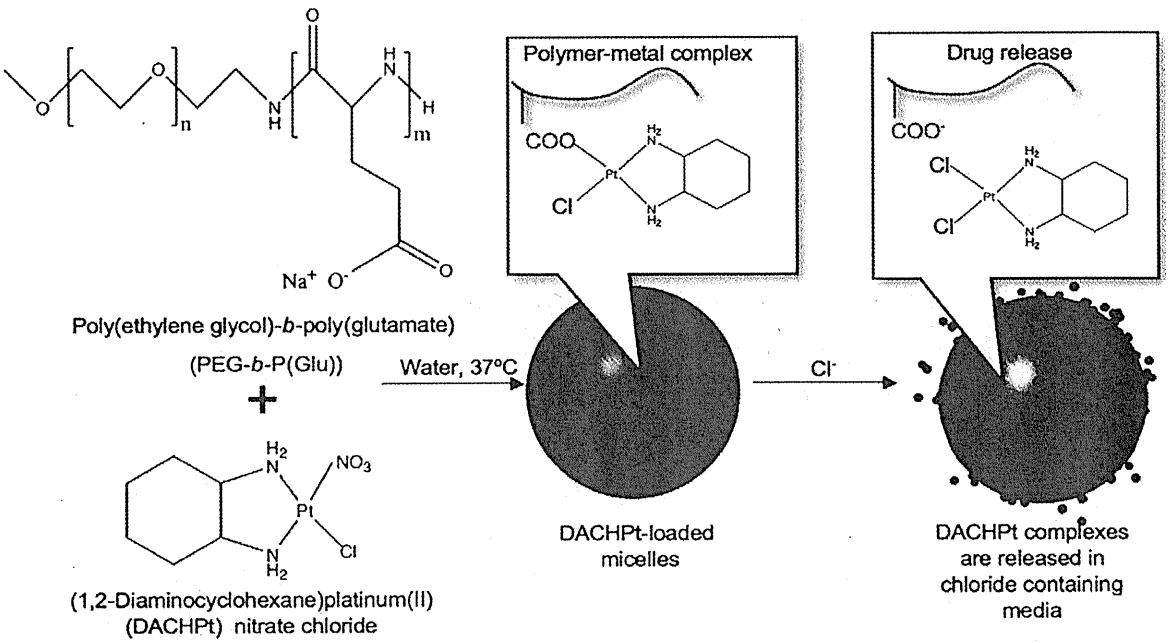


**Fig. 1.** Scheme of the preparation of DACHPt-loaded micelles (DACHPt/m). The micelles are formed by the polymer–metal complex formation between DACHPt and the carboxylic acid moieties in the poly(glutamic acid) backbone. DACHPt is released in a sustained manner as a result of the ligand substitution of the Pt(II) from the carboxylates in the core of the micelles with the chloride ions in the medium.

Please cite this article as: M. Rafi, et al., Polymeric micelles incorporating (1,2-diaminocyclohexane)platinum (II) suppress the growth of orthotopic scirrhous gastric tumors ..., J. Control. Release (2012), doi:10.1016/j.jconrel.2012.01.038

**Table 1**
Fifty-percent cell growth inhibitory concentration ($IC_{50}$) of DACHPt/m and oxaliplatin against human scirrhous gastric cancer OCUM-2-MLN cells.

| Drug | $IC_{50}$ (μM) | |
|---|---|---|
| | 48 h | 72 h |
| DACHPt/m | 20.0 | 12.5 |
| Oxaliplatin | 12.5 | 6.25 |

exchange of DACHPt from the carboxylic groups of p(Glu) to the chloride ions in the media [28]. The 50% cell growth inhibitory concentration ($IC_{50}$) of DACHPt/m was approximately 2-fold higher than that of oxaliplatin (Table 1).

### 3.2. Antitumor activity against bioluminescent orthotopic gastric tumors

OCUM-2MLN cells stably expressing luciferase gene (OCUM-2MLN-Luc) were prepared by the lentiviral transfection. The bioluminescent signal of OCUM-2MLN-Luc after the addition of luciferin was measured by IVIS (Supplementary Fig. S2). As the light glowing from the cells increased linearly with cell density (Supplementary Fig. S2), we can use the light intensity of OCUM-2MLN-Luc to quantify the tumor burden.

The antitumor activity of oxaliplatin and DACHPt/m was studied in mice bearing orthotopic OCUM-2MLN-Luc tumors that have

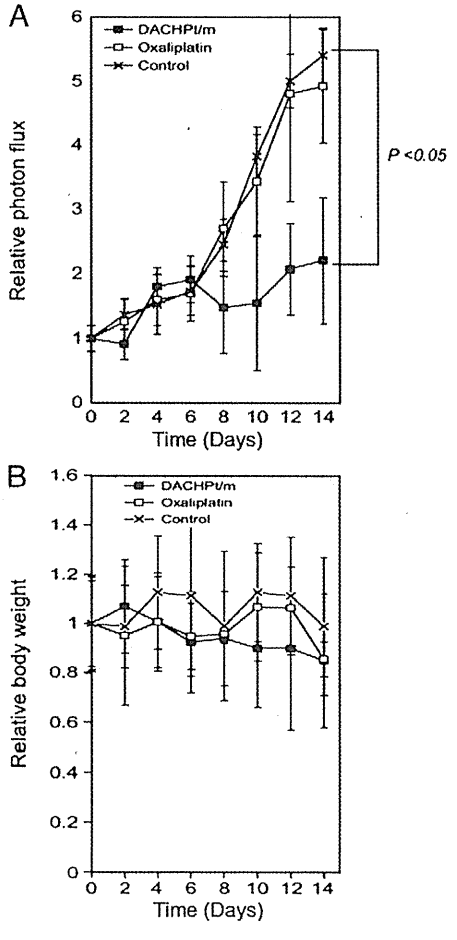


**Fig. 2.** Antitumor activity of oxaliplatin and DACHPt/m against bioluminescent OCUM-2-MLN-Luc orthotopic gastric cancer. A, Relative photon flux from the tumors after the injection of saline, oxaliplatin 8 mg/kg and DACHPt/m 4 mg/kg on days 0, 2 and 4. B, Relative body weight of the mice. Data are expressed as a mean ± SE ($n = 5$).

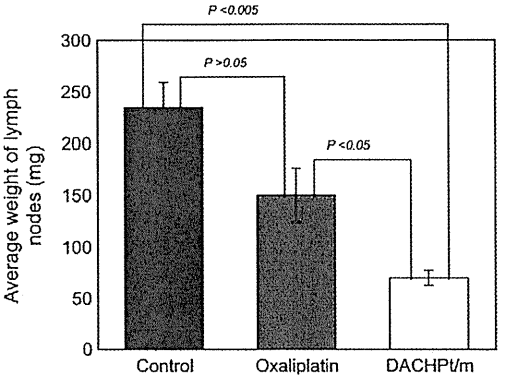


**Fig. 3.** Weight of the metastatic lymph nodes at the end of the antitumor activity experiment (day 14). Data are expressed as a mean ± SE ($n = 5$).

already developed metastasis to the lymph nodes. The mice were treated intravenously 3 times at 0, 2 and 4 days with oxaliplatin at 8 mg/kg or DACHPt/m at 4 mg/kg on a Pt basis. The photon flux (photons per second) from the bioluminescent tumors was assessed by IVIS every second day. Consequently, oxaliplatin failed to show any antitumor effect against the OCUM-2MLN-Luc tumors as the photon flux of oxaliplatin-treated mice was comparable to that of untreated mice (Fig. 2A). In contrast, the mice treated with DACHPt/m showed significantly lower relative photon flux compared with untreated and oxaliplatin-treated mice (Fig. 2A) without significant body weight loss (Fig. 2B), indicating a significant antitumor activity against the orthotopic gastric tumors.

### 3.3. Growth inhibition of lymph node metastasis

At the end of the antitumor activity study, the mice were sacrificed and the metastatic lymph nodes were collected and weighed. As shown in Fig. 3, the weights of the lymph nodes in DACHPt/m-treated mice were approximately four and two times lower than those in untreated mice and oxaliplatin-treated mice, respectively, suggesting that DACHPt/m might effectively inhibit the growth of the metastatic lymph nodes and their efficacy might surpass that of oxaliplatin.

### 3.4. Biodistribution of DACHPt/m in orthotopic gastric tumors and metastatic lymph nodes

DACHPt/m gradually accumulated in the orthotopic tumors due to the EPR effect, achieving approximately 10% of injected dose per gram of tumor tissue at 24 h (Fig. 4A). The tumor accumulation at 24 h for DACHPt/m was 6 times higher than oxaliplatin (Fig. 4A). DACHPt/m also showed enhanced accumulation in sentinel and distant metastatic lymph nodes (Fig. 4B and C). The effective accumulation of DACHPt/m in the metastatic lymph nodes may account for their effective growth inhibition of lymphatic metastasis.

The *in vivo* distribution of fluorescent-labeled DACHPt/m was assessed by fluorescent imaging of the whole body of tumor-bearing mice. Twenty-four hours after intravenous injection of fluorescent-labeled DACHPt/m, intense fluorescence signal was detected at the tumor site, suggesting the selective accumulation of DACHPt/m in the orthotopic tumors (Fig. 5A). In addition, mice were sacrificed and the tumor, metastatic lymph nodes and organs (i.e., spleen, liver and kidneys) were imaged *ex vivo* (Fig. 5B). The high fluorescence signal of the micelles in the tumor and metastatic lymph nodes indicates the ability of the micelles to target the scirrhous gastric tumors and their lymphatic metastases.

Please cite this article as: M. Rafi, et al., Polymeric micelles incorporating (1,2-diaminocyclohexane)platinum (II) suppress the growth of orthotopic scirrhous gastric tumors ..., J. Control. Release (2012), doi:10.1016/j.jconrel.2012.01.038

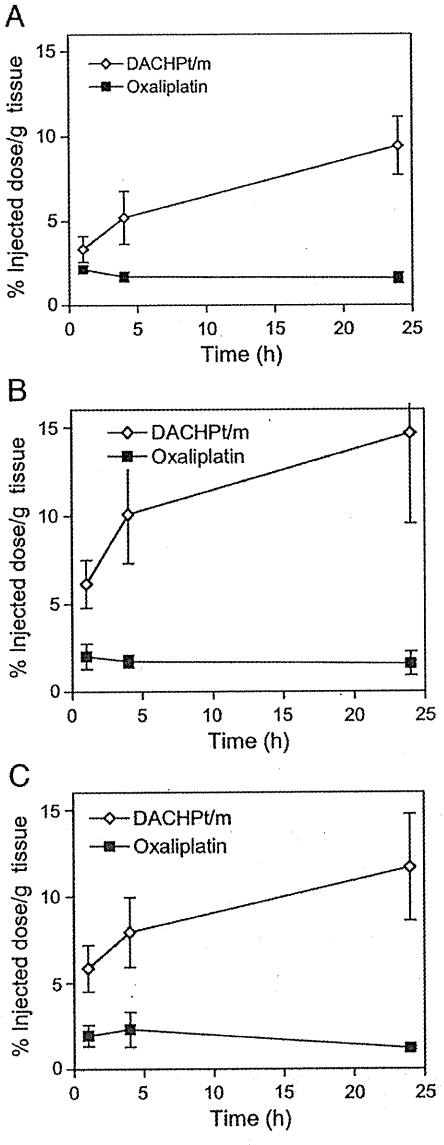


**Fig. 4.** Accumulation of oxaliplatin and DACHPt/m in OCUM-2-MLN-Luc orthotopic tumors and lymph node metastasis. A, Orthotopic tumor. B, Primary metastatic lymph node (sentinel lymph node). C, Secondary metastatic lymph node. Data are expressed as a mean ± SE ($n = 5$).

### *3.5. Microdistribution of fluorescent-labeled DACHPt/m in orthotopic tumors and metastastic lymph nodes*

Firstly, the histology of OCUM-2MLN tumors was examined by H&E staining (Fig. 6A). These tumors present poorly differentiated characteristics with hypovascularity and extensive stromal fibrosis of gastric cancers [9]. The microdistribution of the fluorescent-labeled DACHPt/m in the tissue sections of the orthotopic gastric tumors was assessed by fluorescence microscopy. The nucleus of the cells in the whole tissue sections were stained with Hoechst (Fig. 6B, blue) while the tumors regions were stained by using anti-CD326 antibody (Fig. 6B, green), which recognizes the human epithelial antigen (HEA). The colocalization of the fluorescent-labeled DACHPt/m (Fig. 6B, magenta) with the CD326-stained cancer cells (Fig. 6B, green) suggests the homogeneous accumulation of the micelles in the tumor tissue (Fig. 6B). Moreover, the blood vessels, marked with anti-PECAM-1 antibody, were not detectable within the tumor (Fig. 6C, green), suggesting the hypovascular nature of the tumors. Also, the lymphatic vessels, marked with anti-LIVE-1 antibody, were not detected inside the tumor tissue (Fig. 6C, blue). In OCUM-2MLN tumor model, the cancer cells exhibit tumor invasion into peritumoral lymphatic vessels and spread along the lymphatic vessels in the gastric wall to the regional lymph nodes [33]. The fluorescence of the micelles was detected in the tumor sections even at the regions distant from the blood vessels (Fig. 6C, magenta), suggesting the deep penetration of DACHPt/m within the tumor tissue.

The H&E staining of the metastatic lymph nodes (Fig. 7A) indicated the abnormal anatomy of the lymph node due to the tumor growth. Fluorescent signal from the micelles was found to be colocalized with cancer cells, stained by CD326, in the metastatic lymph nodes, suggesting that micelles deeply penetrate into the metastases in the lymph nodes (Fig. 7B). Additionally, the lymphatic tissue and blood vessels were stained with anti-LYVE-1 and anti-PECAM-1 antibodies, respectively (Fig. 7C). LYVE-1-positive lymphatic tissue was mainly found in the periphery of the tumor in the lymph node (Fig. 7C, blue). Fluorescent-labeled micelles were found to accumulate within the tumoral region of the metastatic lymph nodes (Fig. 7C, magenta).

It is assumed that polymeric micelles from the circulation may reach the lymph nodes either through the lymphatic vessels or blood vessels. Meanwhile, the fluorescent micelles were not detected in healthy lymph nodes (Supplementary Fig. S4). The histological examinations of the enhanced accumulation of DACHPt/m in the metastatic lymph nodes are quite consistent with the significant growth inhibition of lymph node metastasis observed in DACHPt/m treated animals (Fig. 3).

## 4. Discussion

In the present study, we examined the targeting ability of DACHPt/m against the orthotopic model of scirrhous gastric cancer (SGC) from OCUM-2MLN cells, which is accompanied with very high rate of lymph node metastasis [30–31]. The metastasis to the lymph nodes is an important indicator for the staging of SGC and a determinant for the prognosis [35–36]. Here, we have successfully demonstrated that systemically administered DACHPt/m can target both orthotopic scirrhous gastric tumors and their lymphatic metastasis, achieving a remarkable inhibitory effect on their growth.

The biodistribution study revealed that the micelles significantly accumulated in the tumors and the metastatic lymph nodes (Figs. 5 and 6) while showing appreciably lower accumulation in organs or healthy lymph nodes (Fig. **5** and Fig.**S4**). The accumulation of DACHPt/m in the orthotopic OCUM-2MLN tumors might be related to the passive targeting based on the EPR effect. However, we have previously reported that doxorubicin-loaded polymeric micelles with 65-nm diameter showed poor accumulation and reduced efficacy against orthotopic OCUM-2MLN tumors [9]. Regarding such discrepancy, we assume that a relatively small size (30 nm) of DACHPt/m should be important for effective extravasation and tumor penetration in orthotopic OCUM-2MLN tumors. Recently, we have studied the size effect of DACHPt/m in subcutaneous human pancreatic adenocarcinoma BxPC3 tumors [29], which share histological characteristics with OCUM-2MLN tumors, such as sparse formation of blood vessels and very thick fibrotic stroma [30–31]. Accordingly, DACHPt/m with 30-nm diameter effectively extravasated and penetrated in the pancreatic tumors while DACHPt/m with diameter larger than 50-nm remained in the perivascular areas of the tumors [29]. Based on these observations, we preliminarily studied the size effect of DACHPt/m in an orthotopic OCUM-2MLN tumor model in this study (Supplementary Information). As shown in Supplementary Fig. **S3**, 30-nm DACHPt/m showed potent antitumor efficacy and enhanced tumor accumulation against gastric tumors, whereas 70-nm DACHPt/m failed to exhibit significant antitumor effect and showed

Please cite this article as: M. Rafi, et al., Polymeric micelles incorporating (1,2-diaminocyclohexane)platinum (II) suppress the growth of orthotopic scirrhous gastric tumors ..., J. Control. Release (2012), doi:10.1016/j.jconrel.2012.01.038

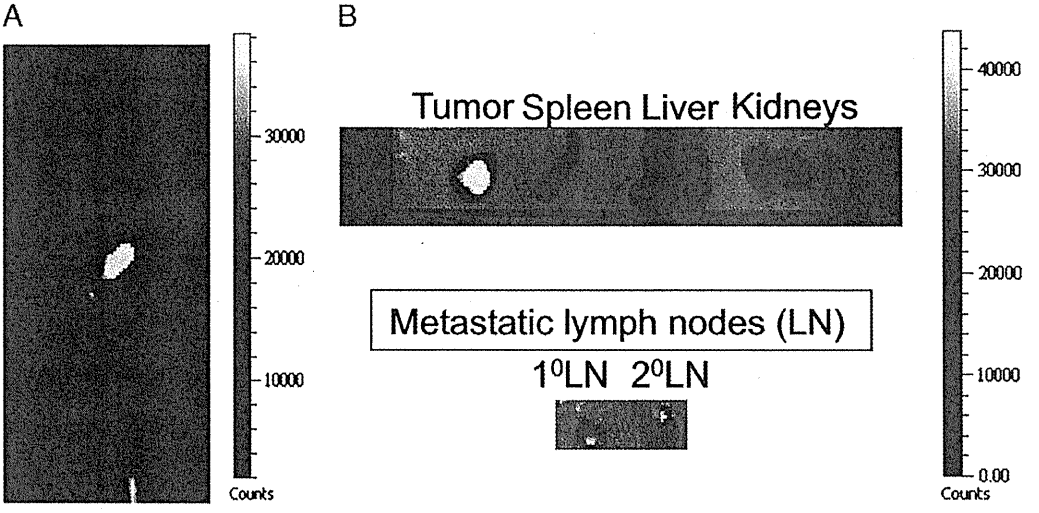


**Fig. 5.** Biodistribution of Alexa 680-labeled DACHPt/m. A, Whole body near infrared (NIR) fluorescent image of orthotopic OCUM-2-MLN-Luc tumor-bearing mouse 24 h after the injection of Alexa 680-labeled DACHPt/m. The micelles are detected specifically at the tumor site. B, *Ex vivo* fluorescent imaging of orthotopic tumor, organs and metastatic lymph nodes.

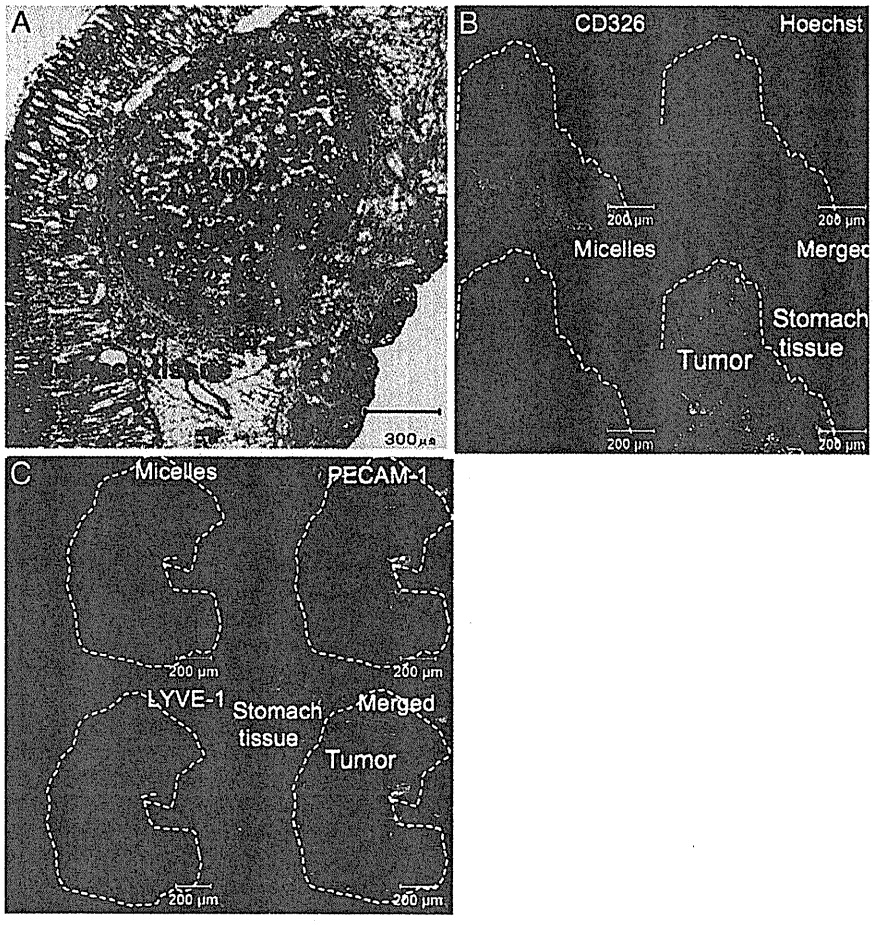


**Fig. 6.** Histological analysis of orthotopic OCUM-2-MLN-Luc and microdistribution of fluorescent labeled DACHPt/m. A, H&E staining of orthotopic OCUM-2-MLN-Luc tumor sections. B, Immunofluorescence microscopy of gastric cancer cells (CD326, green) and Alexa 594-labeled DACHPt/m (magenta) in orthotopic OCUM-2-MLN-Luc tumors. The cells nuclei were stained with Hoechst 33342 (blue). C, Microdistribution of Alexa 594-labeled DACHPt/m (micelles, magenta), blood vessels (PECAM-1, green) and lymphatic vessels (LYVE-1, blue) in orthotopic OCUM-2-MLN-Luc tumors determined by immunofluorescence microscopy.

Please cite this article as: M. Rafi, et al., Polymeric micelles incorporating (1,2-diaminocyclohexane)platinum (II) suppress the growth of orthotopic scirrhous gastric tumors ..., J. Control. Release (2012), doi:10.1016/j.jconrel.2012.01.038

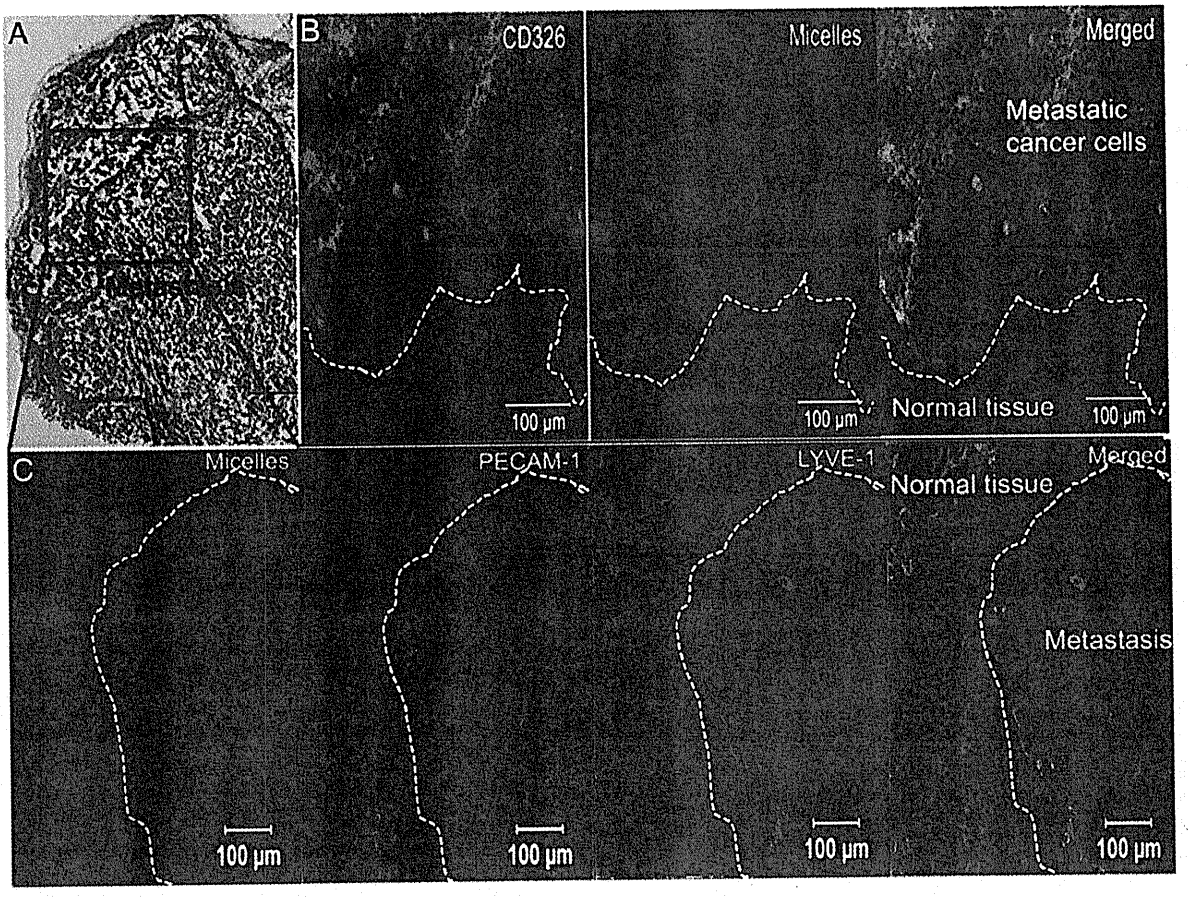


**Fig. 7.** Histological analysis of metastatic lymph nodes and microdistribution of fluorescent labeled DACHPt/m. A, H&E staining of metastatic lymph node. B, Immunofluorescence microscopy of gastric cancer cells (CD326, green) and Alexa 594-labeled DACHPt/m (micelles, magenta) in the metastatic lymph nodes. C, Microdistribution of Alexa 594-DACHPt/m (micelles, magenta), blood vessels (PECAM-1, green) and lymphatic vessels (LYVE-1, blue) in metastatic lymph nodes (Inset of A) determined by immunofluorescence microscopy.

poor tumor accumulation. These results are consistent with the aforementioned assumption that effective properties of DACHPt/m against a scirrhous gastric cancer model may be attributed to their relatively small size.

The observation of DACHPt/m accumulation into the fibrous OCUM-2MLN tumor here is apparently consistent with the scheme of EPR effect. On the other hand, the mechanisms of the accumulation of the micelles in the metastatic lymph nodes remain to be clarified yet. Two mechanisms for the accumulation of the micelles in the metastatic lymph nodes may be proposed: (i) the micelles accumulate in the orthotopic tumors, followed by migration and accumulation in the metastatic lymph nodes via the lymphatic vessels, (ii) the micelles can directly accumulate in the metastatic lymph nodes via blood vessels in the metastatic niche probably due to the enhanced permeability of these blood vessels. Regarding the former mechanism, intratumorally-injected nanocarriers have been demonstrated to accumulate in the metastatic lymph nodes [16,17,37,38]. Also, Harisinghani et al. reported in patients that systemically injected superparamagnetic iron oxide nanoparticles (SPION) accumulate in the metastatic lymph nodes [39]. This phenomenon was explained by accumulation of SPION in solid tumors, followed by their uptake by tumor macrophages, which migrate to metastatic lymph nodes [39]. The detailed mechanisms underlying the accumulation of the micelles in the metastatic lymph nodes are under investigation and will be reported elsewhere.

The targeting capability of the micelles to scirrhous gastric tumors and their metastatic lymph nodes could be applied not only for treatment but also for diagnosis. A variety of contrast agents, including fluorescent probes, MRI or PET contrast agents [5] can be incorporated into the micellar structure. Thus, primary scirrhous tumors and nodal involvement may be directly observed by non-invasive imaging. Moreover, the combination of therapy and imaging within single micelles may allow the evaluation of the therapeutic response, offering an emerging concept of theranostic nanomedicines [5,27].

In conclusion, our results highlight that systemically injected DACHPt/m can extravasate and penetrate in orthotopic scirrhous gastric tumors and lymph node metastasis, eliciting significantly potent antitumor activity. Enhanced drug delivery to the lymph node metastasis by polymeric micelles can improve the morbidity of the patients with SGC. DACHPt/m can also be useful for the adjuvant therapy of SGC, that is, the administration of the micelles before surgery, by improving the lymph node status while controlling the tumor volume, which may lead to the downgrading of unresectable scirrhous gastric cancer. Moreover, control of distant lymph node metastasis by DACHPt/m can impede further dissemination of the disease. Our findings suggest the high potential of systemically administered nanocarriers for the treatment of scirrhous gastric cancer as well as lymph node metastasis.

## Acknowledgments

This study was supported by Funding Program for World-Leading Innovative R&D on Science and Technology (FIRST Program) from the Japan Society for the Promotion of Science (JSPS) and Grants-in-Aid

for Scientific Research from the Japanese Ministry of Health, Labour, and Welfare (MHLW).

## Appendix A. Supplementary data

Supplementary data to this article can be found online at doi:10.1016/j.jconrel.2012.01.038.

## References

[1] R. Duncan, The dawning era of polymer therapeutics, Nat. Rev. Drug Discov. 2 (2003) 347–360.
[2] M.E. Davis, Z. Chen, D. Shin, Nanoparticle therapeutics: an emerging treatment modality for cancer, Nat. Rev. Drug Discov. 7 (2008) 771–782.
[3] K. Kataoka, A. Harada, Y. Nagasaki, Block copolymer micelles for drug delivery: design, characterization and biological significance, Adv. Drug Deliv. Rev. 47 (2001) 113–131.
[4] N. Nishiyama, K. Kataoka, Current state, achievements, and future prospects of polymeric micelles as nanocarriers for drug and gene delivery, Pharmacol. Ther. 112 (2006) 630–648.
[5] H. Cabral, N. Nishiyama, K. Kataoka, Supramolecular nanodevices: from design validation to theranostic nanomedicine, Acc. Chem. Res. 44 (2011) 999–1008.
[6] Y. Matsumura, H. Maeda, A new concept for macromolecular therapeutics in cancer chemotherapy: mechanism of tumoritropic accumulation of proteins and the antitumor agent Smancs, Cancer Res. 46 (1986) 6387–6392.
[7] J.J. Gottlieb, K. Washenik, A. Chachoua, A. Friedman-Kien, Treatment of classic Kaposi's sarcoma with liposomal encapsulated doxorubicin, Lancet 350 (1997) 1363–1364.
[8] W.J. Gradishar, S. Tjulandin, N. Davidson, H. Shaw, N. Desai, P. Bhar, M. Hawkins, J. O'Shaughnessy, Phase III trial of nanoparticle albumin-bound paclitaxel compared with polyethylated castor oil-based paclitaxel in women with breast cancer, J. Clin. Oncol. 23 (2005) 7794–7803.
[9] M.R. Kano, Y. Bae, C. Iwata, Y. Morishita, M. Yashiro, M. Oka, T. Fujii, A. Komuro, K. Kiyono, M. Kaminishi, K. Hirakawa, Y. Ouchi, N. Nishiyama, K. Kataoka, K. Miyazono, Improvement of cancer-targeting therapy, using nanocarriers for intractable solid tumors by inhibition of TGF-β signaling, Proc. Natl. Acad. Sci. U. S. A. 104 (2007) 3460–3465.
[10] M.R. Kano, Y. Komuta, C. Iwata, M. Oka, Y.T. Shirai, Y. Morishita, Y. Ouchi, K. Kataoka, K. Miyanozo, Comparison of the effects of the kinase inhibitors imatinib, sorafenib, and transforming growth factor-β receptor inhibitor on extravasation of nanoparticles from neovasculature, Cancer Sci. 100 (2009) 173–180.
[11] K.D. Crew, A.I. Neugut, Epidemiology of gastric cancer, World J. Gastroenterol. 12 (2006) 354–362.
[12] E. Otsuji, Y. Kuriu, K. Okamoto, T. Ochiai, D. Ichikawa, A. Hagiwara, H. Yamagishi, Outcome of surgical treatment for patients with scirrhous carcinoma of the stomach, Am. J. Surg. 188 (2004) 327–332.
[13] Japanese Gastric, Cancer A Japanese classification of gastric carcinoma—2nd English Edition, Gastric Cancer 1 (1998) 10–24.
[14] Y. Hippo, M. Yashiro, M. Ishii, H. Taniguchi, S. Tsutumi, K. Hirakawa, T. Kosama, H. Aburatani, Differential gene expression profiles of scirrhous gastric cancer cells with high metastatic potential to peritoneum or lymph nodes, Cancer Res. 61 (2001) 889–895.
[15] Y. Maehara, Y. Emi, H. Baba, Y. Adachi, K. Akazawa, Y. Ichiyoshi, K. Sugimachi, Recurrences and related characteristics of gastric cancer, Br. J. Cancer 74 (1996) 975–979.
[16] A. Hagiwara, T. Takahashi, K. Sawai, C. Sakakura, M. Shirasu, M. Ohgaki, T. Imanishi, J. Yamasaki, Y. Takemoto, N. Kageyama, Selective drug delivery to peri-tumoral region and regional lymphatics by local injection of aclarubicin adsorbed on activated carbon particles in patients with breast cancer—a pilot study, Anticancer Drugs 8 (1997) 666–670.
[17] C. Oussoren, G. Storm, Liposomes to target the lymphatics by subcutaneous administration, Adv. Drug Deliv. Rev. 50 (2001) 143–156.
[18] P. Hirnle, Targeted introduction of substances into the lymph nodes for endolymphatic therapy, in: Stanley P.L. Leong (Ed.), Cancer metastasis and the lymphovascular system: basis for rational therapy, Springer, 2007, p. 101.
[19] K. Yamagata, K. Kumagai, K. Shimizu, K. Masuo, Y. Nishida, A. Yasui, Gastrointestinal cancer metastasis and lymphogenous spread: viewpoint of animal models of lymphatic obstruction, Jpn. J. Clin. Oncol. 28 (1998) 104–106.
[20] Y. Matsumura, T. Hamaguchi, T. Ura, K. Muro, Y. Yamada, Y. Shimada, K. Shirao, T. Okusaka, H. Ueno, M. Ikeda, N. Watanabe, Phase I clinical trial and pharmacokinetic evaluation of NK911, a micelle-encapsulated doxorubicin, Br. J. Cancer 91 (2004) 1775–1781.
[21] T. Hamaguchi, K. Kato, H. Yasui, C. Morizane, M. Ikeda, H. Ueno, K. Muro, Y. Yamada, T. Okusuka, K. Shirao, Y. Shimada, H. Nakahama, Y. Matsumura, A phase I and pharmacokinetic study of NK105, a paclitaxel-incorporating micellar nanoparticle formulation, Br. J. Cancer 97 (2007) 170–176.
[22] Y. Matsumura, K. Kataoka, Preclinical and clinical studies of anticancer agent-incorporating polymer micelles, Cancer Sci. 100 (2009) 572–579.
[23] Y. Matsumura, Preclinical and clinical studies of NK012, an SN-38-incorporating polymeric micelles, which is designed based on EPR effect, Adv. Drug Deliv. Rev. 63 (2010) 184–192.
[24] R. Plummer, R.H. Wilson, H. Calvert, A.V. Boddy, M. Griffin, J. Sludden, M.J. Tilby, M. Eatock, D.G. Pearson, C.J. Ottley, Y. Matsumura, K. Kataoka, T. Nishiya, A Phase I clinical study of cisplatin-incorporated polymeric micelles (NC-6004) in patients with solid tumours, Br. J. Cancer 104 (2011) 593–598.
[25] H. Cabral, N. Nishiyama, S. Okazaki, H. Koyama, K. Kataoka, Preparation and biological properties of dichloro(1,2-diaminocyclohexane)platinum (II) (DACHPt)-loaded polymeric micelles, J. Control. Release 101 (2005) 223–232.
[26] H. Cabral, N. Nishiyama, K. Kataoka, Optimization of (1,2-diamino-cyclohexane) platinum(II)-loaded polymeric micelles directed to improved tumour targeting and enhanced antitumour activity, J. Control. Release 121 (2007) 146–155.
[27] S. Kaida, H. Cabral, M. Kumagai, A. Kishimura, Y. Terada, M. Sekino, I. Aoki, N. Nishiyama, T. Tani, K. Kataoka, Visible drug delivery by supramolecular nanocarriers directing to single-platformed diagnosis and therapy of pancreatic tumor model, Cancer Res. 70 (2010) 7031–7041.
[28] M. Murakami, H. Cabral, Y. Matsumoto, S. Wu, M.R. Kano, T. Yamori, N. Nishiyama, K. Kataoka, Improving drug potency and efficacy by nanocarrier-mediated subcellular targeting, Sci. Transl. Med. 3 (2011) 64ra2.
[29] H. Cabral, Y. Matsumoto, K. Mizuno, Q. Chen, M. Murakami, M. Kimura, Y. Terada, M.R. Kano, K. Miyazono, M. Uesaka, N. Nishiyama, K. Kataoka, Accumulation of sub-100nm polymeric micelles in poorly permeable tumours depends on size, Nat. Nanotech. 6 (2011) 815–823.
[30] T. Fujihara, T. Sawada, K. Hirakawa, Y.S. Chung, M. Yashiro, T. Inoue, M. Sowa, Establishment of lymph node metastatic model for human gastric cancer in nude mice and analysis of factors associated with metastasis, Clin. Exp. Metastasis 16 (1998) 389–398.
[31] M. Yashiro, K. Hirakawa, Cancer–stromal interactions in scirrhous gastric carcinoma, Cancer Microenviron. 3 (2010) 127–135.
[32] K. Shibuya, J. Shirakawa, T. Kameyama, S. Honda, S. Tahara Hanaoka, A. Miyamoto, M. Onodera, T. Sumida, H. Nakauchi, H. Miyoshi, A. Shibuya, CD226 (DNAM-1) is involved in lymphocyte function-associated antigen 1 costimulatory signal for naive T cell differentiation and proliferation, J. Exp. Med. 198 (2003) 1829–1839.
[33] C. Iwata, M.R. Kano, A. Komuro, M. Oka, K. Kiyono, E. Johansson, Y. Morishita, M. Yashiro, K. Hirakawa, M. Kaminishi, K. Miyazono, Inhibition of cyclooxygenase-2 suppresses lymph node metastasis via reduction of lymphangiogenesis, Cancer Res. 67 (2007) 10181–10189.
[34] D.E. Jenkins, Y. Oei, Y.S. Hornig, S.F. Yu, J. Dusich, T. Purchio, P.R. Contag, Bioluminescent imaging (BLI) to improve and refine traditional murine models of tumor growth and metastasis, Clin. Exp. Metastasis. 20 (2003) 733–744.
[35] M.S. Karpeh, L. Leon, D. Klimstra, M.F. Brennan, Lymph node staging in gastric cancer: is location more important than Number? An analysis of 1,038 patients, Ann. Surg. 232 (2000) 362–371.
[36] C.Y. Chen CY, C.W. Wu, S.S. Lo, M.C. Hsieh, W.Y. Lui, K.H. Shen, Peritoneal carcinomatosis and lymph node metastasis are prognostic indicators in patients with Borrmann type IV gastric carcinoma, Hepatogastroenterology 49 (2002) 874–877.
[37] C. Oussoren, G. Storm, Lymphatic uptake and biodistribution of liposomes after subcutaneous injection: III. Influence of surface modification with poly(ethyleneglycol), Pharm. Res. 14 (1997) 1479–1484.
[38] G. Luo, X. Yu, C. Jin, F. Yang, D. Fu, J. Long, J. Xu, C. Zhan, W. Lu, LyP-1-conjugated nanoparticles for targeting drug delivery to lymphatic metastatic tumors, Int. J. Pharm. 385 (2010) 150–156.
[39] M.G. Harisinghani, J. Barentsz, P.F. Hahn, W.M. Deserno, S. Tabatabaei, C.H. van de Kaa, J. de la Rosette, R. Weissleder, Noninvasive detection of clinically occult lymph-node metastases in prostate cancer, N. Engl. J. Med. 348 (2003) 2491–2499.

nature nanotechnology

ARTICLES

PUBLISHED ONLINE: 23 OCTOBER 2011 | DOI: 10.1038/NNANO.2011.166

# Accumulation of sub-100 nm polymeric micelles in poorly permeable tumours depends on size

H. Cabral[1], Y. Matsumoto[2], K. Mizuno[3], Q. Chen[4], M. Murakami[2], M. Kimura[2], Y. Terada[5], M. R. Kano[6], K. Miyazono[6,7], M. Uesaka[3,7], N. Nishiyama[2,7]* and K. Kataoka[1,2,4,7]*

**A major goal in cancer research is to develop carriers that can deliver drugs effectively and without side effects. Liposomal and particulate carriers with diameters of ~100 nm have been widely used to improve the distribution and tumour accumulation of cancer drugs, but so far they have only been effective for treating highly permeable tumours. Here, we compare the accumulation and effectiveness of different sizes of long-circulating, drug-loaded polymeric micelles (with diameters of 30, 50, 70 and 100 nm) in both highly and poorly permeable tumours. All the polymer micelles penetrated highly permeable tumours in mice, but only the 30 nm micelles could penetrate poorly permeable pancreatic tumours to achieve an antitumour effect. We also showed that the penetration and efficacy of the larger micelles could be enhanced by using a transforming growth factor-β inhibitor to increase the permeability of the tumours.**

Targeting tumours with long-circulating nanomedicines, such as poly(ethylene glycol)-modified liposomes and polymeric micelles[1–6], is a promising strategy in systemic cancer treatment. These materials accumulate in solid tumours through the enhanced permeability and retention (EPR) effect[7], which is characterized by leaky blood vessels and an impaired lymphatic drainage in tumour tissues[7]. Compared with free drug, nanomedicines accumulate in solid tumours more easily and selectively and therefore offer better antitumour activity[8–15]. Several nanomedicines, including Doxil and Abraxane (diameters of 90 and 130 nm, respectively), have shown significant antitumour activity in highly vascularized tumours such as Kaposi's sarcoma and breast cancer, and have been approved for clinical use[16,17]. However, because Doxil and other nanomedicines with diameters larger than 100 nm have shown limited penetration and accumulation in tumours with hypovascular and hypopermeable characteristics[18–20] (such as intractable pancreatic tumours[18,20]), nanomedicines in the sub-100 nm range are now regarded as being more important in the study of tumour penetration[21,22].

Polymeric micelles (self-assemblies of block copolymers) are promising long-circulating nanomedicines[5,6,8–10] and have been widely studied in preclinical and clinical trials[13,14,23]. Clinical studies have demonstrated that polymeric micelles of poly(ethylene glycol)–*b*-poly(amino acid) copolymers incorporating paclitaxel, SN-38, doxorubicin or cisplatin drugs can reduce the toxic side effects of the loaded drugs[13,14,24,25] while maintaining appreciable antitumour efficacy. Micelles containing paclitaxel and SN-38 have been reported to reduce the size of tumours in patients with advanced cancers of the breast and pancreas[13,14]. The dense poly(ethylene glycol) (PEG) shell of the micelles prevents protein adsorption and recognition by the phagocyte system, and this prolongs blood circulation, a prerequisite for enhanced tumour accumulation based on the EPR effect. Moreover, with these micelles, the size (including those in the sub-100 nm range), stability, loading capacity and release kinetics of the drugs can be modulated by engineering the constituent block copolymers[5,6]. Here, we examine whether a series of micellar nanomedicines that have diameters less than 100 nm and that carry the potent tumoricidal agent 1,2-diaminocyclohexane-platinum(II) (DACHPt) (the parent complex of oxaliplatin) can accumulate and penetrate poorly permeable pancreatic tumours. Our results show that the size of the nanomedicines critically affects the penetration and efficacy of the drugs in the tumours. Larger micelles that could not penetrate otherwise, could penetrate once the permeability of the tumours was improved by administering a transforming growth factor-β inhibitor.

## Characterization of DACHPt-loaded micelles

DACHPt-loaded micelles (DACHPt/m) were spontaneously formed from the interaction of the platinum of DACHPt and the carboxylic moieties of PEG–*b*-poly(glutamic acid) (PEG–*b*-P(Glu)) copolymer and the poly(glutamic acid) (P(Glu)) homopolymer in water (Fig. 1a)[10,26,27]. Differently sized DACHPt/m were synthesized by controlling the mixing ratio of P(Glu) from the homopolymer and the P(Glu) portion of PEG–*b*-P(Glu) (Fig. 1b). As the ratio of P(Glu) in the homopolymer and P(Glu) in the copolymer increases, the size of the micelles increases. Thus, the size of DACHPt/m ranged from 30 nm without the addition of P(Glu) homopolymer to more than 100 nm, while maintaining a narrow distribution as determined by dynamic light scattering (DLS) measurements and transmission electron microscopy (TEM) observations (Table 1 and Supplementary Fig. S1, respectively). Note that DLS measurements provide the hydrodynamic diameter of the DACHPt/m, and TEM gives the core diameter of the micelles, so the difference between the hydrodynamic diameter and the core size gives an indication of the thickness of the PEG shell of the micelles.

[1]Department of Bioengineering, Graduate School of Engineering, The University of Tokyo, 7-3-1 Hongo, Bunkyo-ku, Tokyo, 113-8656, Japan, [2]Center for Disease Biology and Integrative Medicine, Graduate School of Medicine, The University of Tokyo, 7-3-1 Hongo, Bunkyo-ku, Tokyo 113-0033, Japan, [3]Department of Nuclear Engineering and Management, Graduate School of Engineering, The University of Tokyo, 7-3-1 Hongo, Bunkyo-ku, Tokyo 113-8656, Japan, [4]Department of Materials Engineering, Graduate School of Engineering, The University of Tokyo, 7-3-1 Hongo, Bunkyo-ku, Tokyo 113-8656, Japan, [5]SPring 8, JASRI, 1-1-1 Kouto, Sayo-cho, Sayo-gun, Hyogo 679-5198, Japan, [6]Department of Molecular Pathology, Graduate School of Medicine, The University of Tokyo, 7-3-1 Hongo, Bunkyo-ku, Tokyo 113-0033, Japan, [7]Center for NanoBio Integration (CNBI), The University of Tokyo, 7-3-1 Hongo, Bunkyo-ku, Tokyo 113-8656, Japan. *e-mail: nishiyama@bmw.t.u-tokyo.ac.jp; kataoka@bmw.t.u-tokyo.ac.jp